Title
Dissecting the Role of R-loops in DNA Damage and Repair

Author
Amon, Jeremy David

Publication Date
2016

Peer reviewed|Thesis/dissertation

Dissecting the Role of R-loops in DNA Damage and Repair

By

Jeremy David Amon

A dissertation submitted in partial satisfaction of the
requirements for the degree of
Doctor of Philosophy

in

Molecular and Cell Biology

in the

Graduate Division

of the

University of California, Berkeley

Committee in charge:

Professor Douglas Koshland, chair
Professor Kathleen Collins
Professor Gary Karpen
Professor Daniel Zilberman

Summer 2016

Abstract

Dissecting the Role of R-loops in DNA Damage and Repair

by

Jeremy David Amon

Doctor of Philosophy in Molecular and Cell Biology

University of California, Berkeley

Professor Douglas Koshland, Chair

R-loops, three-stranded structures that form when transcripts hybridize to chromosomal DNA, are potent agents of genome instability. This instability has been explained by the ability of R-loops to induce DNA damage. Here, we show that persistent R-loops also compromise DNA repair. Depleting endogenous RNase H activity impairs R-loop removal in budding yeast, causing DNA damage that occurs preferentially in the repetitive ribosomal DNA locus (rDNA). We analyzed the repair kinetics of this damage and identified mutants that modulate repair. Our results indicate that persistent R-loops in the rDNA induce damage that is slowly repaired by break-induced replication (BIR). Furthermore, R-loop induced BIR at the rDNA leads to lethal repair intermediates when RNA polymerase I elongation is compromised. We present a model to explain how removal of R-loops by RNase H is critical in ensuring the efficient repair of R-loop induced DNA damage by pathways other than BIR.

To my grandparents:
Emil (ז"ל), Eda,
Albert (ז"ל), and Mat (ז"ל)

Table of Contents

Acknowledgements

I would first like to thank the members of the Koshland lab, all of whom have helped me in countless ways throughout my PhD. I have learned more than I thought possible from Thomas, Aaron, Fred, Weijia, Vinny, Hugo, Gamze, Michelle, Brett, Rebecca, Jeremiah, Skylar, Kristian, Ryan, and Heba. A special thank you goes to team hybrid – Anjali, Lorenzo, Lamia, and Steven – who in addition to guiding my general growth as a scientist have made direct intellectual contributions to the research reported here. To the entire lab, past and present, thank you for making this a friendly, challenging, rigorous, and fun place to work. Thank you for being so open and sharing, for providing endless feedback and help with experiments, and for giving me so many reasons to laugh.

Many thanks to Doug, who has been a tireless mentor to me. Thank you for always leaving your door open, both literally and metaphorically. Thank you for teaching me how to think carefully about experiments and see all the possible ways a result could be interpreted. Thank you for pushing me to be a better scientist, your patience in waiting for me to become one, and your willingness to give me second chances and not give up on me when my progress has been slow. Most of all, thank you for your dedication to your ideals. In the face of cynicism and cutthroat competition, thank you for always reminding me that it's important to take the time to be an active member of the scientific community, to share good ideas instead of hoard them, and that it's better to be cautious and correct than flashy and famous.

A very special thank you goes to Alex Muir and Alex Wu for being partners in absurdity, bowling buddies, fellow buffet and music video aficionados, scientific sounding boards, career advisors, and two of my closest friends. I am continually inspired by your empathy, your brilliant minds, the work you do, and the hilarity you create.

To all my Bay Area friends: thank you for the music, the swimming, the dinners, the jokes, the adventures, the company, and the support. Cameron, Heather, Chuck, Samantha, Nikki, Cindy, Caroline, Julia, Sushant, Candice, Julio, Zach, Drew, and Rachel, I will miss you dearly. I could not have made it this long and through so many challenges without feeling like I was part of some kind of family. Thank you for being that family and for making Berkeley feel a bit like home.

Joe Friedman, thanks for calling and keeping me company when I'm in lab late at night. I always look forward to our chats, and you have picked me up after many long days and failed experiments.

Lastly, I would like to thank Avi, Sabrina, Mom and Dad. It feels trite and almost disingenuous to thank you for the love and support you have provided me with over the years. I suppose that's because it feels too obvious, and it's therefore too easy for me to thank you for them. So instead, I will say thank you for making your love and support so commonplace and so ordinary that I almost take them for granted. Know that I think of you daily, miss you constantly, and love you always.

Chapter I. Introduction

Genomic instability is a balancing act. On one hand, high rates of mutation and chromosome rearrangements can have severe, detrimental effects on cells and organisms. On the other, low levels of mutation and chromosomal rearrangements are essential for an organism's long-term evolutionary success. Generally speaking, rates of mutation in mitotically dividing eukaryotic cells are kept remarkably low – on the order of 10^{-10} mutations per base pair per division in the yeast *Saccharomyces cerevisiae*, by some estimates [1]. However, it is important to note that a wide range of genetic alterations can fall under the category of genomic instability. Small-scale instability includes single nucleotide polymorphisms and microsatellite repeat expansions and contractions. Large-scale instability includes loss-of-heterozygosity (LOH), aneuploidy, and gross chromosomal rearrangements (GCRs) such as terminal deletions, translocations, and inversions.

This low rate of mutation represents a complex interplay between many physical, chemical, and biological factors. On a cellular level, the overall rate of genomic instability can be broadly defined as the rate at which DNA damage occurs minus the rate at which the damage is repaired through one of several highly conserved pathways. Increases in the rate of initial DNA damage and decreases in the efficacy of subsequent DNA repair can both increase the overall rate of genome instability. For example, a point mutation could be the result of an improperly matched base during DNA replication (the initial damage event), and a failure of the mismatch repair system to revert this base to the proper one (the subsequent failure of repair). Alternatively, a terminal deletion event involving the loss of part of one arm of a chromosome could be the result of an ionizing radiation-induced double-strand break (DSB) in G1 followed by the failure of the non-homologous end-joining pathway to reattach the distal end of the chromosome.

These are two of many possible examples – a large number of damaging events, both endogenous and exogenous, can contribute to DNA instability, and for every class of DNA damage, there is one or several corresponding pathways of DNA repair that could potentially undo the damage. Single base mutations and aberrations, such as those caused by UV irradiation, errors in replication, and reactive oxidative species are processed through several pathways including the nucleotide excision repair, base-excision repair, and mismatch repair pathways (reviewed in [2,3]). Larger-scale mutations such as GCRs are often caused by DSBs in DNA, and are processed through non-homologous end joining or one of several homology-directed repair pathways.

Homology-directed double-strand break repair

DSBs are a particularly dangerous event for a cell – even a single DSB can be lethal if it goes unrepaired [4]. It is therefore of utmost importance to repair a DSB as efficiently as possible. In the presence of homologous sequences that can serve as

templates for DSB repair, the yeast *Saccharomyces cerevisiae* overwhelmingly utilizes recombination-based methods of DNA repair (homologous recombination, or HR, is reviewed in [5]). These methods can be summarized as three pathways that serve as distinct options for DSB repair: gene-conversion (GC), single strand annealing (SSA), and break-induced replication (BIR). All three pathways preferentially occur in S- or G2/M phases, which ensures the presence of sister chromatids that serve as repair templates [6]. Common to all three pathways is the early step of 5' to 3' resection, which creates 3' single strand overhangs and commits the cell to a homology-directed repair pathway (reviewed in [7,8]).

GC appears to be the pathway of choice for yeast, as it is the only option of the three that can result in the complete maintenance of all genetic information after a DSB. After resection, single-stranded 3' overhangs are coated with the strand-exchange protein Rad51, and both ends of the DSB find and invade a homologous sequence, thereby forming a D-loop. A short stretch of DNA is then replicated, often using the synthesis-dependent strand-annealing mechanism, but sometimes using a double-Holiday junction intermediate [9].

If a proper D-loop involving capture of both ends of a DSB does not occur, SSA may take over. As the cell searches for homology, resection continues at a rate of about 4 kb per hour [10,11]. If at any point this resection uncovers homologous sequences, for example, between two of the many Ty retrotransposons found throughout the yeast genome, these sequences can anneal, deleting the intervening region [12].

BIR is perhaps the most enigmatic of the three HR pathways. If only a single end of a DSB is captured by homology, the cell will wait at the so-called "recombination execution checkpoint" [13]. Then, if after several hours the second strand is not captured in the proper orientation, the cell will initiate extremely processive replication that can copy the length of entire chromosomes using error-prone polymerases (reviewed in [14]).

Transcription-associated genome instability

One ubiquitous endogenous source of genome instability is transcription. Transcription was first implicated as a driver of genome instability in the early 1970s, when the rate of reversion of certain bacterial Lac^- mutants was shown to increase two-fold upon induction of the *lac* operon [15]. The ability to increase rates of reversion by inducing transcription has since been corroborated across many species, including T7 phage [16], *Salmonella typhimurium* [17], *Escherichia coli* [18,19], and *S. cerevisiae* [20]. Notably, the non-transcribed strand was shown to be particularly vulnerable to mutation, implying that it was single-stranded for long enough to be exposed to hydrolytic agents [18].

DNA recombination has also been associated with transcription. Initial studies showed that transcript elongation increased rates of phage λ recombination [21]. In yeast, it was shown that a fragment of the ribosomal DNA (rDNA) locus termed *HOT1* (although this name has largely fallen out of use in favor of more specific discussion of elements within the *HOT1* locus – see section on the rDNA locus) was a hotspot for

recombination, and could stimulate recombination when inserted into ectopic loci [22]. The precise requirements for the orientation of promoter regions within *HOT1* suggested that transcription was required for this recombinogenic activity. Indeed, RNA polymerase I, which regulates rDNA transcription, was shown to be necessary for stimulating recombination [23,24].

This stimulatory effect on recombination was shown to be a general result of transcription and not specific to any one polymerase. RNA polymerase II transcription was shown to increase recombination of a locus under the control of a GAL promoter in *S. cerevisiae* [25], as well as in mammalian cells [26]. Lastly, experiments performed in yeast showed that transcription by RNA polymerase III could also induce recombination as well [27].

It is of note that all of these analyses of transcription-induced recombination tested the ability of direct repeats, such as those found at the rDNA, to recombine with each other. These recombination events, which involve the loss of intervening sequences, imply the presence of a DSB intermediate. Consistent with this possibility, recombination events driven at a single locus by either transcription or the HO endonuclease have similar dependencies for DSB-repair genes such as *RAD51, RAD52,* and *RAD59* [28]. While this study was largely correlational, it supported the idea that transcription could increase DSBs and Rad52-dependent recombination events.

R-loops form in vivo

An important clue to understanding the mechanisms behind transcription-associated mutagenesis came with the discovery that transcription-associated mutations appear asymmetrically on DNA [18,29]. The observed mutations were largely C-to-T transitions, which occur when cytosine is deaminated to uracil, either spontaneously or enzymatically. Uracil found in DNA is then paired with adenine during DNA replication, which in turn is paired to thiamine during the following replication cycle or upon the induction of a repair pathway (reviewed in [30]). While it was clear that these increased rates of mutation were happening at transcribed regions, it was unknown whether this strand-specific bias was indeed a result of an increased mutation rate on the non-transcribed strand or was an artifact of transcription-coupled DNA repair, which is known to predominantly affect the transcribed strand (reviewed in [31,32]). It was argued that the mutational signature was more consistent with former [33]. Together with data showing that the rate of cytosine deamination in single stranded DNA is approximately 140-fold higher than in double stranded DNA [34], it was suggested that active transcription formed stretches of single-stranded DNA vulnerable to deamination.

Normally, active RNA polymerases form a short, 8-9 base-pair DNA:RNA hybrid contained within the polymerase complex [35]. This hybrid is disengaged as the polymerase translocates and the nascent RNA strand and its DNA template exit through separate pores [36]. The two strands of DNA then re-anneal behind the polymerase. There is therefore a short-lived, small stretch of single-stranded DNA that moves with the polymerase, but this stretch appears to be largely protected by the complex [37]. Thus,

the question of how chemically vulnerable ssDNA is produced is not satisfactorily answered by the displaced non-transcribed strand.

As an RNA polymerase translocates, positive supercoiling builds up in the double-stranded DNA ahead of it and negative supercoiling accrues behind [38]. It had been proposed that the under-wound region of DNA behind the polymerase could be invaded by a nascent RNA strand, which would then stably base-pair with its template. This three-stranded structure, involving a DNA:RNA hybrid and a single strand of DNA, is known as an R-loop. Indeed, R-loops can be created in the negatively supercoiled region of an *in vitro* transcribed plasmid [39]. Surprisingly, DNA:RNA hybrids created in vitro appear to be more stable than their DNA:DNA or RNA:RNA counterparts, and therefore form relatively stable structures that are not easily displaced [40,41].

The first evidence for R-loops forming *in vivo* came in specific biological instances that were not widely generalizable to transcription as a whole. A long, transcriptionally dependent DNA:RNA hybrid was shown to form at a conserved mitochondrial DNA sequence and was later shown to initiate DNA replication [42-45]. Additionally, the immunoglobulin locus was shown to have a persistent, ~140 bp DNA:RNA hybrid that was dependent on transcription [46-48]. Interestingly, R-loops were shown to have functional significance at this locus in the process of class switch recombination, the method by which immunoglobulin heavy chains are switched to different isotypes (reviewed in [49]).

A turning point in the study of *in vivo* R-loops came with the study of the effects of the RNases H on genome stability. RNase H1 and H2, reviewed in more detail below, are two endogenous ribonucleases that can cleave the RNA moiety of a DNA:RNA hybrid. In a clever series of experiments by Huertas and Aguilera [50], a self-cleaving hammerhead ribozyme was embedded in a direct-repeat recombination system under the control of a *GAL* promoter. When the ribozyme was active, nascent transcripts were cleaved, and hyper-recombination phenotypes caused by active transcription of the locus in an *hpr1*Δ background were dramatically reduced. When RNase H1 was overexpressed in these cells, hyper-recombination was reduced even in the presence of an inactive ribozyme. This argued that co-transcriptionally formed R-loops were responsible for at least some transcription-associated recombination events.

Later, in an important series of experiments by Li and Manley [51], it was shown that depletion of splicing factor ASF/SF2 results in genomic instability. High molecular weight DNA structures from these cells were shown to be R-loops using a bisulfite sequencing method. Extracted genomic DNA was exposed to sodium bisulfite, which deaminated exposed cytosines on single stranded DNA to uracil. Sequencing revealed asymmetric, ~100 bp stretches of C-to-U conversions only in genomic DNA extracted from cells depleted of ASF/SF2. When RNase H was overexpressed in these cells, these stretches disappeared. ASF/SF2 was also shown to suppress R-loop formation *in vitro*. Taken together, an RNA splicing factor that acts co-transcriptionally was shown to prevent R-loop formation that could lead to genome instability.

R-loops contribute to genomic instability

That splicing factors and active ribozymes could prevent co-transcriptional R-loop from forming seemed to confirm the "thread back" model of R-loop formation. This also made a set of testable predictions about the interactions between R-loops and RNA processing factors in the nucleus. Factors that bind, process, or otherwise decrease the amount of time a nascent RNA spends in the nucleus near its template should help prevent R-loops and their associated genome instability. Indeed, THO complex mutants involved in RNA export in yeast were shown to have this effect [52-54]. A large number of RNA biogenesis factors, including those involved in transcriptional repression, transcript elongation, RNA degradation, and RNA transport have all been implicated in hybrid formation and RNase H-suppressible genome instability [55]. Additionally, homologous recombination machinery, namely Rad51, has been implicated in creating R-loops, perhaps by encouraging strand invasion or stabilizing triplex structures [56].

In bacteria, where translation is tightly coupled with transcription, translation factors can also play a role in R-loop formation. Here, the ribosome and its associated factors act like the early RNA binding proteins in eukaryotes. Interestingly, the first studies to investigate transcription-associated instability could not distinguish between the roles of transcription and translation [15]. While this question was put to rest when experiments were performed in eukaryotes with spatially distinct transcription and translation [20], active ribosomes were eventually implicated in preventing transcription-associated genome instability in bacteria [57].

The ability of R-loops to induce genome instability has expanded well beyond direct-repeat recombination. Several different forms of genome instability can result in the presence of R-loops. In results highly reminiscent of transcriptional associated mutagenesis experiments, certain DNA-modifying enzymes such as activation-induced cytidine deaminase act at R-loops to induce single nucleotide mutations [58]. High rates of LOH and chromosome loss events were shown to be RNase H suppressible in RNA biogenesis mutants [55]. Lastly, as for direct repeat instability, DSBs were further implicated by genome instability events that can only be explained by breaks in both DNA strands, including recombination at the rDNA locus and terminal deletion events on both natural and synthetic chromosomes [55,59].

Topoisomerase I and R-loops

We have perhaps been remiss in avoiding discussion of topoisomerase I (Top1 in yeast) until this point, as the history of Top1, R-loops, and transcription-associated instability are remarkably intertwined. Top1 is a type I topoisomerase, meaning that it cleaves and covalently attaches to a single strand of DNA, then freely swivels around the unbroken strand, thereby removing tension in double-stranded DNA. More specifically, Top1 is a type IB topoisomerase, which are not found in *E. coli* – bacterial topoisomerases I and III are of type IA and more similar to yeast Top3 (reviewed in [60]). While there are important biochemical differences between type IA and IB

topoisomerases, they have overlapping *in vivo* functions [61], and yeast Top1 is able to fully complement lethal mutants of *E. coli* topoisomerase I [62].

The ability to promote ribosomal RNA transcription was among the first biological functions ascribed to yeast Top1, which is nonetheless nonessential [63]. Additionally, genetic studies involving the loss of a marker embedded in the rDNA locus determined that *TOP1* mutants had dramatically increased rates of rDNA recombination [64]. In retrospect, these two results presaged later transcription-associated recombination and R-loop studies – the absence of a trans-acting factor (in this case, Top1) perturbs transcription, and genomic instability increases. Consistent with this prescient trend, one of the first studies to propose the presence of *in vivo* R-loops did so in *topA* mutants in *E. coli*. It was found that overexpression of RNase H1 could partially suppress the lethality of topoisomerase I null mutants [65]. This led the authors to propose a model in which under-wound DNA was susceptible to invasion by RNA, and that R-loops were, through unknown mechanisms, the cause of the growth deficiencies of Δ*topA* strains.

A random mutagenesis screen for mutants that required Top1 found synthetic interactions with *HPR1*, a gene that was already being studied for its hyper-recombination phenotypes which shortly thereafter would be linked to transcription [66,67]. The screen also found and named Trf4 (topoisomerase one-requiring function), which was later discovered to play a role in suppressing R-loops by degrading nuclear RNA as a member of the TRAMP complex [55]. More specifically, Trf4 is involved in the degradation of ribosomal RNA [68]. Additionally, *TOP1* mutants are synthetically lethal with mutants of *RPA34* and *RPA49*, two non-essential RNA Pol I subunits involved in transcript termination [69,70]. Taken together, topoisomerase I has been shown to be required in a wide array of mutants that are deficient in RNA processing and transcription at the ribosomal locus, and many of these mutants have been linked to genome instability.

In an important series of experiments, Top1 mutants were shown to be synthetically lethal in yeast cells lacking both RNase H1 and RNase H2 (*rnh1*Δ *rnh201*Δ) [71]. Depletion of Top1 in *rnh1*Δ *rnh201*Δ cells using catabolite repression of a GAL promoter resulted in an accumulation of DNA:RNA hybrids over the intergenic sequences found in the rDNA. Furthermore, depletion of Top1 in *rnh1*Δ *rnh201*Δ cells caused RNA pol I pileups at the rDNA, as visualized by electron microscopy of Miller spreads [71]. These phenotypes correlated with a dramatic increase in Rad52-GFP foci that co-localized with the nucleolus [72]. These results suggest that topoisomerase I is partially responsible for preventing hybrid formation, stalled RNA pol I complexes, and the resultant genome stability at the rDNA locus.

Recombination at the ribosomal DNA locus is transcription-dependent

The ribosomal DNA locus is a hotspot for genome rearrangements. This is in part due to its highly repetitive nature. In yeast, approximately 150 copies of a 9.1 kb repeating unit exist in a tandem array on chromosome XII. This repeating unit consists of the large 35S gene, which is transcribed by RNA polymerase I and subsequently processed into several ribosome subunits, and the small 5S gene, which is transcribed by RNA polymerase III (reviewed in [73]). The large number of repeats present at the locus

provides recombination events with an extraordinary amount of homology. This makes the rDNA locus relatively easy to repair – at any part of the cell cycle, even in the absence of a sister chromatid or homologous chromosome, DSBs in the rDNA could theoretically still be repaired using a neighboring repeat through BIR or SSA [74,75]. However, this extensive homology also makes the rDNA particularly recombinogenic. The dangers of high levels of recombination lie in the possibilities of creating deleterious genomic rearrangements or dramatically shrinking or expanding the number of repeats through intra-chromosomal exchanges [76].

The rDNA repeats are therefore maintained by cellular control over several *cis* and *trans* factors that act in concert. The initially identified *HOT1* locus was shown to span two intergenic sequences (IGS1 and IGS2) that lie between the 5S and 35S loci. These sequences contain an ARS for DNA replication initiation, a replication fork barrier, and a bidirectional RNA pol I promoter [22,23]. The replication fork barrier and the associated Fob1 protein work together to stall DNA replication machinery advancing from the ARS. This stalling activity prevents replication from proceeding against the direction of transcription in the neighboring 35S gene, and is required for rDNA repeat expansion and contraction [77]. The bidirectional promoter is also required for repeat expansion and contraction [78]. In the absence of RNA pol I or active transcription at this promoter, the rDNA fails to recombine [79]. Taken together, both transcription and replication pausing are required for recombination at the rDNA.

RNases H1 and H2 have both overlapping and distinct functions

The ribonucleases H were first discovered as an activity present in crude calf thymus extracts that prevented synthesis of RNA on denatured DNA. Further investigation found that these extracts could degrade RNA only when it was bound to single stranded DNA. Following this activity through several rounds of purification resulted in isolation of an enzyme that was then named RNase H, with the 'H' standing for hybrid [80,81]. This was followed by the discovery of a second RNase H activity in calf thymus [82]. RNases H were soon found to exist in organisms in all three domains of life and to be present in two distinct classes.

Type 1 RNases H (*RNH1* in yeast) are the more evolutionary conserved of the two. It most species, they consist of a highly conserved hybrid-binding domain connected through a divergent, unstructured linker of variable length to a highly conserved RNase H domain [83,84]. The hybrid binding domain and linker are thought to allow for processive degradation of RNA found in longer hybrids [85]. Many bacterial species lack the linker and the hybrid-binding domain [86]. In mammals, but not yeast, RNase H1 contains two translation start codons, one of which results in an N-terminal mitochondrial targeting sequence. RNase H1 therefore localizes to both the nucleus and the mitochondria [87,88]. RNase H1-null mutants in mammals are early-embryonic lethal, likely due to failures in mitochondrial DNA replication [87]. Pathological alleles of RNase H1 manifest as neuromuscular disease caused by the aggregation of mitochondrial DNA. This aggregation results in improper DNA segregation and dysfunctional mitochondria [89].

Type 2 RNases H are less conserved but still recognizable between species. In eukaryotes, they consist of three subunits – two divergent accessory subunits that flank a conserved catalytic subunit [90-92]. In yeast, these subunits are coded by the genes *RNH201, RNH202,* and *RNH203,* with *RNH201* being the catalytic subunit [93]. As with RNase H1, null RNase H2 mutants are early-embryonic lethal in mice [94,95]. In humans, hypomorphic mutants in all three RNase H2 subunits cause a severe encephalopathy known as Aicardi-Goutières syndrome [96]. The precise pathology of this syndrome remains unknown, but symptoms mimic a congenital infection and are hypothesized to manifest when DNA:RNA hybrid species activate the immune system [97].

In addition to being able to hydrolyze long DNA:RNA hybrids, RNase H2 is uniquely capable of excising single ribonucleotides that are incorporated into DNA [98-100]. In contrast, RNase H1 requires a DNA:RNA hybrid with at least four ribonucleotides for activity [83,101]. Ribonucleotides appear to be accidentally incorporated into the genome with surprising frequency and have been shown to cause genome instability [102,103]. These instability events appear to be suppressible by RNase H2 acting in concert with flap endonucleases and the post-replication repair pathway [104,105]. When RNase H2 fails to clear these misincorporated ribonucleotides, the end result is often small, 2-5 bp deletions as a result of a "messy" alternative clean-up by Top1 [106,107].

Despite the severe phenotypes of mutants in mammals, neither RNase H1 nor RNase H2 are essential in yeast, alone or in combination. When both are mutated (*rnh1*Δ *rnh201*Δ), there is an increase in the persistence of R-loops and a resultant increase in genome instability [55]. This would suggest than in regards to their ability to resolve R-loops, the two enzymes have overlapping functions. This may be largely true, but recent studies have shown that they have different activities in the cell. First, deletion of RNase H2, but not H1, appears to increase persistence of hybrids at certain genomic loci and LOH events [59,108]. Second, careful analysis of R-loop induced instability on chromosome III has shown that RNase H2 plays the major role in suppressing LOH events chromosome wide, while RNase H1 is responsible for suppressing recombination at a specific hotspot (Zimmer and Koshland, in preparation). These studies point to the possibility that RNase H2 is a "general" RNase H, resolving R-loops genome wide, and RNase H1 is a "specific" RNase H, assigned to certain problematic loci.

RNA polymerase backtracking – a third RNase H?

A seldom-mentioned third RNase H activity was initially found in calf thymus and was shown to associate with RNA polymerase I [109]. This activity is partially separable from the polymerase complex – RNase H activity was associated both with RNA pol I subunits A49 and A34.5, and with the remaining RNA pol I complex lacking subunits A49/34.5 [110,111]. Many years later, this activity was confounded with an ability of RNA pol I to cleave nascent transcripts in a 3' to 5' manner [112]. A similar activity was found in RNA pol II [113]. This confusion was clarified by providing the polymerase with the appropriate substrate – a DNA-RNA hybrid with a 3' RNA

overhang. This assembled the polymerase into a "backtracked" state, which led to efficient 3' to 5' RNase activity [114]. This backtracked state can occur when an RNA polymerase translocates by several base pairs in the opposite direction of transcription, perhaps after encountering a physical block, and the nascent transcript exits through a specialized pore in the complex. Cleavage activity was less efficient in the absence of the A49/34.5 subunits and was completely absent after the deletion of the C-terminal domain of the non-essential A12.2 subunit (Rpa12 in yeast). This subunit is structurally similar to the TFIIS subunit of RNA pol II, which is also involved in cleaving backtracked substrates [115]. Together with evidence in bacteria that backtracked RNA polymerases encourage R-loop induced DSBs, this suggests an exciting possibility that backtracking resolution and transcript termination play an important role in preventing R-loop induced instability [57].

S9.6 antibody and R-loop mapping efforts

A particular boon to the study of DNA:RNA hybrids came with the advent of the S9.6 monoclonal antibody. This antibody was initially characterized in 1986, but aside from a few immunological studies, was quickly forgotten [116,117]. Decades later, the antibody was unearthed and further characterized by researchers hoping to find an immunochemical approach to detecting RNA hybridization to DNA microarrays [118]. Given the unique structure of DNA:RNA hybrids – similar to, but distinct from A-form DNA (reviewed in [119]) – the antibody proved to be highly specific to this particular nucleic acid duplex. There appeared to be no sequence specificity, and it could only recognize hybrids of at least 15 nucleotides in length. It should be noted that this antibody has been shown to have some cross-reactivity with double-stranded RNA, but at a lower specificity [120,121].

The S9.6 antibody has been used extensively to show cytological staining of R-loops under different genetic conditions. Several studies have now gone a step further and have used this antibody in chromatin immunoprecipitation-like experiments to determine precise genetic loci of DNA:RNA hybridization [122-124]. These studies found many R-loop associated regions, but had several technical issues that called some of their conclusions into question. Namely, the presence or absence of the RNases H appeared to have little effect on genome-wide DNA:RNA hybrid abundance. More detailed studies using improved methodology were therefore performed with markedly improved signal-to-noise ratios [108]. RNase H sensitive R-loops were found at approximately 800 regions in wild-type cells, along with very high abundance in the rDNA, Ty retrotransposons, and telomeres. This high-resolution map will prove to be a valuable resource in pinpointing loci where R-loop induced instability occurs. Indeed, one such location has already been found on chromosome III (Zimmer and Koshland, in preparation).

Mechanisms of R-loop dependent genome rearrangements

The rDNA provides a striking example of transcription-induced instability, and suggests a potential model for how R-loops can lead to DSBs. Before we proceed however, it is important to note that there is currently no data showing the direct involvement of R-loops in the process of rDNA repeat expansion and contraction. We and others have concluded that R-loop instability occurs at the rDNA locus – an abundance of R-loops accumulate at the rDNA [108], recombination events occur in the rDNA repeats [55,56], and RNA pol I mutants can suppress R-loop induced instability events ([72], this study). However, whether or not the specific process of Fob1-, RFB-, and transcription-dependent expansion and contraction of the rDNA repeats is dependent on a R-loop has not been shown. Additionally, whether instances of R-loop induced rDNA instability are similar to these expansion and contraction events, and thereby dependent on the Fob1/RFB machinery, has yet to be seen. The proper set of experiments to test this, currently underway in our lab, involve genetic manipulation of the RNases H in assays for rDNA repeat and expansion, and conversely, manipulation of Fob1 in assays for R-loop induced instability.

The ability of a stalled DNA polymerase, in concert with transcription, to induce direct-repeat recombination events suggests that collisions between replication and transcription machinery may play a role in generating R-loop induced instability. Replication-transcription collisions have been known to occur *in vivo* since they were first observed in *E. coli* [125]. Since then, collisions have been observed at many genomic loci and in many species (reviewed in [126]). Furthermore, these collisions have been linked to genome instability and recombination [127,128]. However, while replication-transcription collisions appear to be a source of transcriptionally induced instability, few studies support the hypothesis that R-loops can cause these types of collisions.

Perhaps the strongest evidence of a link between replication-transcription collisions, DSBs, and R-loops has been shown in bacteria. In an elegant series of experiments, Dutta et al. measured DSBs on a plasmid-based system that allowed them to differentiate between co-directional and head-on collisions between replication and transcription complexes. Surprisingly, they found that co-directional collisions, and not head-on collisions, cause DSBs. These DSBs were attributable to replication fork collisions with backtracked RNA polymerase complexes, and were suppressible by RNase H, indicating the presence of an R-loop behind the transcription complex [57]. Taken together, the authors proposed a model in which an active replisome collides with a DNA:RNA hybrid created or stabilized by a backtracked RNA polymerase, thereby forming a DSB.

Still, the precise mechanisms by which the DSBs were formed could not be explained. The process by which R-loop dependent collisions are converted to genomic instability events is therefore still not well understood. For possible mechanisms, we turn to literature surrounding the production of DSBs by stalled replication forks (reviewed in[129]). In one potential model, single-stranded DNA at the branch of a stalled replication fork may be hydrolyzed spontaneously or by a structure-specific nuclease. This has precedence in mammals, where the endonuclease Mus81 has been shown to

create DSBs in order to restart replication forks through homologous recombination pathways [130]. However, no such endonuclease has yet been found that contributes to R-loop induced genome instability. In another potential model, R-loops cause single-stranded nicks or gaps that are left in DNA until S-phase, when the replication machinery runs off the nicked template and creates a DSB. This process may occur in UV-nicked DNA, but has been difficult to prove conclusively [131].

We have only discussed models by which R-loops interfere with the DNA replication machinery. These are the models favored in the field, but we note that the necessity of DNA replication in R-loop induced instability has not been thoroughly shown. In fact, some evidence exists that R-loops can generate DNA damage independently of replication. In a particularly curious set of results, R-loop dependent genome instability was seen in stationary, non-dividing *E. coli* [132]. This points to the possibility that R-loop induced instability could occur in mechanisms not involving collisions with replication forks.

While progress on how R-loops form DSBs has been made, much remains unknown about how R-loops cause genome instability. Indeed, the entire focus of the field has been on how R-loops cause genome instability by inducing DNA damage. Here, we explore a new concept that R-loops may generate genome instability not only by inducing damage by also by modulating its repair. Additionally, regardless of the mechanisms by which the initial DNA damage events occur, no evidence for the involvement of specific repair pathways has yet been put forth. Thus, our overall understanding of R-loop generated instability is largely incomplete. In subsequent chapters, we investigate the effects that R-loops have on DNA repair.

References

1. Lang GI, Murray AW. Estimating the per-base-pair mutation rate in the yeast Saccharomyces cerevisiae. Genetics. Genetics; 2008;178: 67–82. doi:10.1534/genetics.107.071506

2. Marteijn JA, Lans H, Vermeulen W, Hoeijmakers JHJ. Understanding nucleotide excision repair and its roles in cancer and ageing. Nat Rev Mol Cell Biol. 2014;15: 465–481. doi:10.1038/nrm3822

3. Li G-M. Mechanisms and functions of DNA mismatch repair. Cell Res. 2008;18: 85–98. doi:10.1038/cr.2007.115

4. Bennett CB, Lewis AL, Baldwin KK, Resnick MA. Lethality induced by a single site-specific double-strand break in a dispensable yeast plasmid. Proceedings of the National Academy of Sciences of the United States of America. National Academy of Sciences; 1993;90: 5613–5617.

5. Pâques F, Haber JE. Multiple pathways of recombination induced by double-strand breaks in Saccharomyces cerevisiae. Microbiol Mol Biol Rev. 1999;63: 349–404.

6. Ira G, Pellicioli A, Balijja A, Wang X, Fiorani S, Carotenuto W, et al. DNA end resection, homologous recombination and DNA damage checkpoint activation require CDK1. Nature. 2004;431: 1011–1017. doi:10.1038/nature02964

7. Kass EM, Jasin M. Collaboration and competition between DNA double-strand break repair pathways. FEBS Lett. 2010;584: 3703–3708. doi:10.1016/j.febslet.2010.07.057

8. Symington LS, Gautier J. Double-strand break end resection and repair pathway choice. Annu Rev Genet. 2011;45: 247–271. doi:10.1146/annurev-genet-110410-132435

9. Ira G, Satory D, Haber JE. Conservative inheritance of newly synthesized DNA in double-strand break-induced gene conversion. Molecular and Cellular Biology. American Society for Microbiology; 2006;26: 9424–9429. doi:10.1128/MCB.01654-06

10. Fishman-Lobell J, Rudin N, Haber JE. Two alternative pathways of double-strand break repair that are kinetically separable and independently modulated. Molecular and Cellular Biology. American Society for Microbiology (ASM); 1992;12: 1292–1303.

11. Zhu Z, Chung W-H, Shim EY, Lee SE, Ira G. Sgs1 helicase and two nucleases

Dna2 and Exo1 resect DNA double-strand break ends. Cell. 2008;134: 981–994. doi:10.1016/j.cell.2008.08.037

12. Hoang ML, Tan FJ, Lai DC, Celniker SE, Hoskins RA, Dunham MJ, et al. Competitive repair by naturally dispersed repetitive DNA during non-allelic homologous recombination. PLoS Genet. Public Library of Science; 2010;6: e1001228. doi:10.1371/journal.pgen.1001228

13. Jain S, Sugawara N, Lydeard J, Vaze M, Tanguy Le Gac N, Haber JE. A recombination execution checkpoint regulates the choice of homologous recombination pathway during DNA double-strand break repair. Genes & Development. Cold Spring Harbor Lab; 2009;23: 291–303. doi:10.1101/gad.1751209

14. Anand RP, Lovett ST, Haber JE. Break-induced DNA replication. Cold Spring Harb Perspect Biol. Cold Spring Harbor Lab; 2013;5: a010397. doi:10.1101/cshperspect.a010397

15. Herman RK, Dworkin NB. Effect of gene induction on the rate of mutagenesis by ICR-191 in Escherichia coli. J Bacteriol. 1971;106: 543–550.

16. Beletskii A, Grigoriev A, Joyce S, Bhagwat AS. Mutations induced by bacteriophage T7 RNA polymerase and their effects on the composition of the T7 genome. J Mol Biol. 2000;300: 1057–1065. doi:10.1006/jmbi.2000.3944

17. Savić DJ, Kanazir DT. The effect of a histidine operator-constitutive mutation on UV-induced mutability within the histidine operon of Salmonella typhimurium. Mol Gen Genet. 1972;118: 45–50.

18. Beletskii A, Bhagwat AS. Transcription-induced mutations: increase in C to T mutations in the nontranscribed strand during transcription in Escherichia coli. Proceedings of the National Academy of Sciences of the United States of America. 1996;93: 13919–13924.

19. Wright BE, Longacre A, Reimers JM. Hypermutation in derepressed operons of Escherichia coli K12. Proceedings of the National Academy of Sciences of the United States of America. 1999;96: 5089–5094.

20. Datta A, Jinks-Robertson S. Association of increased spontaneous mutation rates with high levels of transcription in yeast. Science. 1995;268: 1616–1619.

21. Ikeda H, Matsumoto T. Transcription promotes recA-independent recombination mediated by DNA-dependent RNA polymerase in Escherichia coli. Proceedings of the National Academy of Sciences of the United States of America. 1979;76: 4571–4575.

22. Keil RL, Roeder GS. Cis-acting, recombination-stimulating activity in a

fragment of the ribosomal DNA of S. cerevisiae. Cell. 1984;39: 377–386.

23. Voelkel-Meiman K, Keil RL, Roeder GS. Recombination-stimulating sequences in yeast ribosomal DNA correspond to sequences regulating transcription by RNA polymerase I. Cell. 1987;48: 1071–1079.

24. Stewart SE, Roeder GS. Transcription by RNA polymerase I stimulates mitotic recombination in Saccharomyces cerevisiae. Molecular and Cellular Biology. 1989;9: 3464–3472.

25. Thomas BJ, Rothstein R. Elevated recombination rates in transcriptionally active DNA. Cell. 1989;56: 619–630.

26. Nickoloff JA. Transcription enhances intrachromosomal homologous recombination in mammalian cells. Molecular and Cellular Biology. American Society for Microbiology (ASM); 1992;12: 5311–5318.

27. la Loza de MCD, Wellinger RE, Aguilera A. Stimulation of direct-repeat recombination by RNA polymerase III transcription. DNA Repair. 2009;8: 620–626. doi:10.1016/j.dnarep.2008.12.010

28. González-Barrera S, García-Rubio M, Aguilera A. Transcription and double-strand breaks induce similar mitotic recombination events in Saccharomyces cerevisiae. Genetics. Genetics Society of America; 2002;162: 603–614.

29. Fix DF, Glickman BW. Asymmetric cytosine deamination revealed by spontaneous mutational specificity in an Ung- strain of Escherichia coli. Mol Gen Genet. 1987;209: 78–82.

30. Krokan HE, Drabløs F, Slupphaug G. Uracil in DNA--occurrence, consequences and repair. Oncogene. 2002;21: 8935–8948. doi:10.1038/sj.onc.1205996

31. Hanawalt PC, Spivak G. Transcription-coupled DNA repair: two decades of progress and surprises. Nat Rev Mol Cell Biol. 2008;9: 958–970. doi:10.1038/nrm2549

32. Fong YW, Cattoglio C, Tjian R. The Intertwined Rolesof Transcription and Repair Proteins. Mol Cell. Elsevier Inc; 2013;52: 291–302. doi:10.1016/j.molcel.2013.10.018

33. Francino MP, Ochman H. Deamination as the basis of strand-asymmetric evolution in transcribed Escherichia coli sequences. Mol Biol Evol. 2001;18: 1147–1150.

34. Frederico LA, Kunkel TA, Shaw BR. A sensitive genetic assay for the detection of cytosine deamination: determination of rate constants and the activation energy. Biochemistry. 1990;29: 2532–2537.

35. Gnatt AL, Cramer P, Fu J, Bushnell DA, Kornberg RD. Structural basis of transcription: an RNA polymerase II elongation complex at 3.3 A resolution. Science. American Association for the Advancement of Science; 2001;292: 1876–1882. doi:10.1126/science.1059495

36. Westover KD, Bushnell DA, Kornberg RD. Structural basis of transcription: separation of RNA from DNA by RNA polymerase II. Science. American Association for the Advancement of Science; 2004;303: 1014–1016. doi:10.1126/science.1090839

37. Bernecky C, Herzog F, Baumeister W, Plitzko JM, Cramer P. Structure of transcribing mammalian RNA polymerase II. Nature. 2016;529: 551–554. doi:10.1038/nature16482

38. Liu LF, Wang JC. Supercoiling of the DNA template during transcription. Proceedings of the National Academy of Sciences of the United States of America. National Academy of Sciences; 1987;84: 7024–7027.

39. Drolet M, Bi X, Liu LF. Hypernegative supercoiling of the DNA template during transcription elongation in vitro. J Biol Chem. 1994;269: 2068–2074.

40. Roberts RW, Crothers DM. Stability and properties of double and triple helices: dramatic effects of RNA or DNA backbone composition. Science. 1992;258: 1463–1466.

41. Thomas M, White RL, Davis RW. Hybridization of RNA to double-stranded DNA: Formation of R-loops. Proceedings of the National Academy of Sciences of the United States of America. 1976;73: 2294–2298.

42. Xu B, Clayton DA. A persistent RNA-DNA hybrid is formed during transcription at a phylogenetically conserved mitochondrial DNA sequence. Molecular and Cellular Biology. 1995;15: 580–589.

43. Xu B, Clayton DA. RNA-DNA hybrid formation at the human mitochondrial heavy-strand origin ceases at replication start sites: an implication for RNA-DNA hybrids serving as primers. The EMBO Journal. 1996;15: 3135–3143.

44. Lee DY, Clayton DA. Properties of a primer RNA-DNA hybrid at the mouse mitochondrial DNA leading-strand origin of replication. J Biol Chem. 1996;271: 24262–24269.

45. Lee DY, Clayton DA. Initiation of mitochondrial DNA replication by transcription and R-loop processing. J Biol Chem. 1998;273: 30614–30621.

46. Reaban ME, Griffin JA. Induction of RNA-stabilized DNA conformers by transcription of an immunoglobulin switch region. Nature. 1990;348: 342–344. doi:10.1038/348342a0

47. Reaban ME, Lebowitz J, Griffin JA. Transcription induces the formation of a stable RNA.DNA hybrid in the immunoglobulin alpha switch region. J Biol Chem. 1994;269: 21850–21857.

48. Daniels GA, Lieber MR. RNA:DNA complex formation upon transcription of immunoglobulin switch regions: implications for the mechanism and regulation of class switch recombination. Nucleic Acids Research. 1995;23: 5006–5011.

49. Santos-Pereira JM, Aguilera A. R loops: new modulators of genome dynamics and function. Nat Rev Genet. 2015;16: 583–597. doi:10.1038/nrg3961

50. Huertas P, Aguilera A. Cotranscriptionally formed DNA:RNA hybrids mediate transcription elongation impairment and transcription-associated recombination. Mol Cell. 2003;12: 711–721.

51. Li X, Manley JL. Inactivation of the SR protein splicing factor ASF/SF2 results in genomic instability. Cell. 2005;122: 365–378. doi:10.1016/j.cell.2005.06.008

52. Jimeno S, Rondón AG, Luna R, Aguilera A. The yeast THO complex and mRNA export factors link RNA metabolism with transcription and genome instability. The EMBO Journal. EMBO Press; 2002;21: 3526–3535. doi:10.1093/emboj/cdf335

53. Gómez-González B, García-Rubio M, Bermejo R, Gaillard H, Shirahige K, Marín A, et al. Genome-wide function of THO/TREX in active genes prevents R-loop-dependent replication obstacles. The EMBO Journal. 2011;30: 3106–3119. doi:10.1038/emboj.2011.206

54. Dominguez-Sanchez MS, Barroso S, Gómez-González B, Luna R, Aguilera A. Genome instability and transcription elongation impairment in human cells depleted of THO/TREX. PLoS Genet. Public Library of Science; 2011;7: e1002386. doi:10.1371/journal.pgen.1002386

55. Wahba L, Amon JD, Koshland D, Vuica-Ross M. RNase H and multiple RNA biogenesis factors cooperate to prevent RNA:DNA hybrids from generating genome instability. Mol Cell. 2011;44: 978–988. doi:10.1016/j.molcel.2011.10.017

56. Wahba L, Gore SK, Koshland D. The homologous recombination machinery modulates the formation of RNA-DNA hybrids and associated chromosome instability. Elife. 2013;2: e00505. doi:10.7554/eLife.00505

57. Dutta D, Shatalin K, Epshtein V, Gottesman ME, Nudler E. Linking RNA Polymerase Backtracking to Genome Instability in E. coli. Cell. 2011;146: 533–543. doi:10.1016/j.cell.2011.07.034

58. Gómez-González B, Aguilera A. Activation-induced cytidine deaminase action is

strongly stimulated by mutations of the THO complex. Proceedings of the National Academy of Sciences of the United States of America. 2007;104: 8409–8414. doi:10.1073/pnas.0702836104

59. O'Connell K, Jinks-Robertson S, Petes TD. Elevated Genome-Wide Instability in Yeast Mutants Lacking RNase H Activity. Genetics. Genetics; 2015;201: 963–975. doi:10.1534/genetics.115.182725

60. Berger JM. Structure of DNA topoisomerases. Biochim Biophys Acta. 1998;1400: 3–18.

61. Kim RA, Wang JC. Identification of the yeast TOP3 gene product as a single strand-specific DNA topoisomerase. J Biol Chem. 1992;267: 17178–17185.

62. Bjornsti MA, Wang JC. Expression of yeast DNA topoisomerase I can complement a conditional-lethal DNA topoisomerase I mutation in Escherichia coli. Proceedings of the National Academy of Sciences of the United States of America. National Academy of Sciences; 1987;84: 8971–8975.

63. Brill SJ, DiNardo S, Voelkel-Meiman K, Sternglanz R. Need for DNA topoisomerase activity as a swivel for DNA replication for transcription of ribosomal RNA. Nature. 1987;326: 414–416. doi:10.1038/326414a0

64. Christman MF, Dietrich FS, Fink GR. Mitotic recombination in the rDNA of S. cerevisiae is suppressed by the combined action of DNA topoisomerases I and II. Cell. 1988;55: 413–425.

65. Drolet M, Phoenix P, Menzel R, Massé E, Liu LF, Crouch RJ. Overexpression of RNase H partially complements the growth defect of an Escherichia coli delta topA mutant: R-loop formation is a major problem in the absence of DNA topoisomerase I. Proceedings of the National Academy of Sciences of the United States of America. 1995;92: 3526–3530.

66. Santos-Rosa H, Aguilera A. Increase in incidence of chromosome instability and non-conservative recombination between repeats in Saccharomyces cerevisiae hpr1 delta strains. Mol Gen Genet. 1994;245: 224–236.

67. Prado F, Piruat JI, Aguilera A. Recombination between DNA repeats in yeast hpr1delta cells is linked to transcription elongation. The EMBO Journal. EMBO Press; 1997;16: 2826–2835. doi:10.1093/emboj/16.10.2826

68. Houseley J, Kotovic K, Hage El A, Tollervey D. Trf4 targets ncRNAs from telomeric and rDNA spacer regions and functions in rDNA copy number control. The EMBO Journal. 2007;26: 4996–5006. doi:10.1038/sj.emboj.7601921

69. Gadal O, Mariotte-Labarre S, Chedin S, Quemeneur E, Carles C, Sentenac A, et al. A34.5, a nonessential component of yeast RNA polymerase I, cooperates with

subunit A14 and DNA topoisomerase I to produce a functional rRNA synthesis machine. Molecular and Cellular Biology. 1997;17: 1787–1795.

70. Beckouet F, Labarre-Mariotte S, Albert B, Imazawa Y, Werner M, Gadal O, et al. Two RNA polymerase I subunits control the binding and release of Rrn3 during transcription. Molecular and Cellular Biology. American Society for Microbiology; 2008;28: 1596–1605. doi:10.1128/MCB.01464-07

71. Hage El A, French SL, Beyer AL, Tollervey D. Loss of Topoisomerase I leads to R-loop-mediated transcriptional blocks during ribosomal RNA synthesis. Genes & Development. 2010;24: 1546–1558. doi:10.1101/gad.573310

72. Stuckey R, García-Rodríguez N, Aguilera A, Wellinger RE. Role for RNA:DNA hybrids in origin-independent replication priming in a eukaryotic system. Proceedings of the National Academy of Sciences. National Acad Sciences; 2015;112: 5779–5784. doi:10.1073/pnas.1501769112

73. Kobayashi T. Regulation of ribosomal RNA gene copy number and its role in modulating genome integrity and evolutionary adaptability in yeast. Cell Mol Life Sci. SP Birkhäuser Verlag Basel; 2011;68: 1395–1403. doi:10.1007/s00018-010-0613-2

74. Ozenberger BA, Roeder GS. A unique pathway of double-strand break repair operates in tandemly repeated genes. Molecular and Cellular Biology. American Society for Microbiology (ASM); 1991;11: 1222–1231.

75. Sugawara N, Ira G, Haber JE. DNA length dependence of the single-strand annealing pathway and the role of Saccharomyces cerevisiae RAD59 in double-strand break repair. Molecular and Cellular Biology. 2000;20: 5300–5309.

76. Kobayashi T. Strategies to maintain the stability of the ribosomal RNA gene repeats--collaboration of recombination, cohesion, and condensation. Genes Genet Syst. 2006;81: 155–161.

77. Kobayashi T, Heck DJ, Nomura M, Horiuchi T. Expansion and contraction of ribosomal DNA repeats in Saccharomyces cerevisiae: requirement of replication fork blocking (Fob1) protein and the role of RNA polymerase I. Genes & Development. 1998;12: 3821–3830.

78. Kobayashi T, Nomura M, Horiuchi T. Identification of DNA cis elements essential for expansion of ribosomal DNA repeats in Saccharomyces cerevisiae. Molecular and Cellular Biology. American Society for Microbiology; 2001;21: 136–147. doi:10.1128/MCB.21.1.136-147.2001

79. Kobayashi T, Ganley ARD. Recombination regulation by transcription-induced cohesin dissociation in rDNA repeats. Science. American Association for the Advancement of Science; 2005;309: 1581–1584. doi:10.1126/science.1116102

80. Stein H, Hausen P. Enzyme from calf thymus degrading the RNA moiety of DNA-RNA Hybrids: effect on DNA-dependent RNA polymerase. Science. 1969;166: 393–395.

81. Hausen P, Stein H. Ribonuclease H. An enzyme degrading the RNA moiety of DNA-RNA hybrids. Eur J Biochem. 1970;14: 278–283.

82. Büsen W, Hausen P. Distinct ribonuclease H activities in calf thymus. Eur J Biochem. 1975;52: 179–190.

83. Nowotny M, Gaidamakov SA, Crouch RJ, Yang W. Crystal structures of RNase H bound to an RNA/DNA hybrid: substrate specificity and metal-dependent catalysis. Cell. 2005;121: 1005–1016. doi:10.1016/j.cell.2005.04.024

84. Nowotny M, Gaidamakov SA, Ghirlando R, Cerritelli SM, Crouch RJ, Yang W. Structure of human RNase H1 complexed with an RNA/DNA hybrid: insight into HIV reverse transcription. Mol Cell. 2007;28: 264–276. doi:10.1016/j.molcel.2007.08.015

85. Gaidamakov SA, Gorshkova II, Schuck P, Steinbach PJ, Yamada H, Crouch RJ, et al. Eukaryotic RNases H1 act processively by interactions through the duplex RNA-binding domain. Nucleic Acids Research. 2005;33: 2166–2175. doi:10.1093/nar/gki510

86. Kochiwa H, Tomita M, Kanai A. Evolution of ribonuclease H genes in prokaryotes to avoid inheritance of redundant genes. BMC Evol Biol. BioMed Central; 2007;7: 128. doi:10.1186/1471-2148-7-128

87. Cerritelli SM, Frolova EG, Feng C, Grinberg A, Love PE, Crouch RJ. Failure to produce mitochondrial DNA results in embryonic lethality in Rnaseh1 null mice. Mol Cell. 2003;11: 807–815.

88. Wu H, Sun H, Liang X, Lima WF, Crooke ST. Human RNase H1 Is Associated with Protein P32 and Is Involved in Mitochondrial Pre-rRNA Processing. PLoS ONE. 2013;8: e71006. doi:10.1371/journal.pone.0071006

89. Akman G, Desai R, Bailey LJ, Yasukawa T, Dalla Rosa I, Durigon R, et al. Pathological ribonuclease H1 causes R-loop depletion and aberrant DNA segregation in mitochondria. Proceedings of the National Academy of Sciences. National Acad Sciences; 2016;: 201600537. doi:10.1073/pnas.1600537113

90. Shaban NM, Harvey S, Perrino FW, Hollis T. The Structure of the Mammalian RNase H2 Complex Provides Insight into RNA-DNA Hybrid Processing to Prevent Immune Dysfunction. J Biol Chem. 2010;285: 3617–3624.

91. Rychlik MP, Chon H, Cerritelli SM, Klimek P, Crouch RJ, Nowotny M. Crystal structures of RNase H2 in complex with nucleic acid reveal the mechanism of

RNA-DNA junction recognition and cleavage. Mol Cell. 2010;40: 658–670. doi:10.1016/j.molcel.2010.11.001

92. Figiel M, Chon H, Cerritelli SM, Cybulska M, Crouch RJ, Nowotny M. The Structural and Biochemical Characterization of Human RNase H2 Complex Reveals the Molecular Basis for Substrate Recognition and Aicardi-Goutieres Syndrome Defects. Journal of Biological Chemistry. 2011;286: 10540–10550. doi:10.1074/jbc.M110.181974

93. Jeong H-S, Backlund PS, Chen H-C, Karavanov AA, Crouch RJ. RNase H2 of Saccharomyces cerevisiae is a complex of three proteins. Nucleic Acids Research. 2004;32: 407–414. doi:10.1093/nar/gkh209

94. Reijns MAM, Rabe B, Rigby RE, Mill P, Astell KR, Lettice LA, et al. Enzymatic removal of ribonucleotides from DNA is essential for Mammalian genome integrity and development. Cell. 2012;149: 1008–1022. doi:10.1016/j.cell.2012.04.011

95. Hiller B, Achleitner M, Glage S, Naumann R, Behrendt R, Roers A. Mammalian RNase H2 removes ribonucleotides from DNA to maintain genome integrity. Journal of Experimental Medicine. 2012;209: 1419–1426. doi:10.1084/jem.20120876

96. Rice G, Patrick T, Parmar R, Taylor CF, Aeby A, Aicardi J, et al. Clinical and molecular phenotype of Aicardi-Goutieres syndrome. Am J Hum Genet. 2007;81: 713–725. doi:10.1086/521373

97. Crow YJ, Rehwinkel J. Aicardi-Goutieres syndrome and related phenotypes: linking nucleic acid metabolism with autoimmunity. Hum Mol Genet. Oxford University Press; 2009;18: R130–6. doi:10.1093/hmg/ddp293

98. Eder PS, Walder JA. Ribonuclease H from K562 human erythroleukemia cells. Purification, characterization, and substrate specificity. J Biol Chem. 1991;266: 6472–6479.

99. Eder PS, Walder RY, Walder JA. Substrate specificity of human RNase H1 and its role in excision repair of ribose residues misincorporated in DNA. Biochimie. 1993;75: 123–126.

100. Rydberg B, Game J. Excision of misincorporated ribonucleotides in DNA by RNase H (type 2) and FEN-1 in cell-free extracts. Proceedings of the National Academy of Sciences of the United States of America. 2002;99: 16654–16659. doi:10.1073/pnas.262591699

101. Hogrefe HH, Hogrefe RI, Walder RY, Walder JA. Kinetic analysis of Escherichia coli RNase H using DNA-RNA-DNA/DNA substrates. J Biol Chem. 1990;265: 5561–5566.

102. Nick Mcelhinny SA, Watts BE, Kumar D, Watt DL, Lundstrom E-B, Burgers PMJ, et al. Abundant ribonucleotide incorporation into DNA by yeast replicative polymerases. Proceedings of the National Academy of Sciences. 2010;107: 4949–4954. doi:10.1073/pnas.0914857107

103. Mcelhinny SAN, Kumar D, Clark AB, Watt DL, Watts BE, Lundström E-B, et al. Genome instability due to ribonucleotide incorporation into DNA. Nature Chemical Biology. 2010;6: 774–781. doi:10.1038/nchembio.424

104. Lazzaro F, Novarina D, Amara F, Watt DL, Stone JE, Costanzo V, et al. RNase H and Postreplication Repair Protect Cells from Ribonucleotides Incorporated in DNA. Mol Cell. 2012;45: 99–110. doi:10.1016/j.molcel.2011.12.019

105. Sparks JL, Chon H, Cerritelli SM, Kunkel TA, Johansson E, Crouch RJ, et al. RNase H2-Initiated Ribonucleotide Excision Repair. Mol Cell. 2012. doi:10.1016/j.molcel.2012.06.035

106. Kim N, Huang S-YN, Williams JS, Li YC, Clark AB, Cho J-E, et al. Mutagenic Processing of Ribonucleotides in DNA by Yeast Topoisomerase I. Science. 2011;332: 1561–1564.

107. Williams JS, Smith DJ, Marjavaara L, Lujan SA, Chabes A, Kunkel TA. Topoisomerase 1-Mediated Removal of Ribonucleotides from Nascent Leading-Strand DNA. Mol Cell. 2013. doi:10.1016/j.molcel.2012.12.021

108. Wahba L, Costantino L, Tan FJ, Zimmer A, Koshland D. S1-DRIP-seq identifies high expression and polyA tracts as major contributors to R-loop formation. Genes & Development. Cold Spring Harbor Lab; 2016;30: 1327–1338. doi:10.1101/gad.280834.116

109. Huet J, Wyers F, Buhler JM, Sentenac A, Fromageot P. Association of RNase H activity with yeast RNA polymerase A. Nature. 1976;261: 431–433.

110. Huet J, Buhler JM, Sentenac A, Fromageot P. Characterization of ribonuclease H activity associated yeast RNA polymerase A. J Biol Chem. 1977;252: 8848–8855.

111. Iborra F, Huet J, Breant B, Sentenac A, Fromageot P. Identification of two different RNase H activities associated with yeast RNA polymerase A. J Biol Chem. 1979;254: 10920–10924.

112. Tschochner H. A novel RNA polymerase I-dependent RNase activity that shortens nascent transcripts from the 3' end. Proceedings of the National Academy of Sciences of the United States of America. 1996;93: 12914–12919.

113. Labhart P. Transcript cleavage in an RNA polymerase I elongation complex. Evidence for a dissociable activity similar to but distinct from TFIIS. J Biol

Chem. 1997;272: 9055–9061.

114. Kuhn C-D, Geiger SR, Baumli S, Gartmann M, Gerber J, Jennebach S, et al. Functional architecture of RNA polymerase I. Cell. 2007;131: 1260–1272. doi:10.1016/j.cell.2007.10.051

115. Cheung ACM, Cramer P. Structural basis of RNA polymerase II backtracking, arrest and reactivation. Nature. 2011;471: 249–253. doi:10.1038/nature09785

116. Boguslawski SJ, Smith DE, Michalak MA, Mickelson KE, Yehle CO, Patterson WL, et al. Characterization of monoclonal antibody to DNA-RNA and its application to immunodetection of hybrids. 1986;89: 123–130.

117. Casebolt DB, Stephensen CB. Monoclonal antibody solution hybridization assay for detection of mouse hepatitis virus infection. J Clin Microbiol. American Society for Microbiology (ASM); 1992;30: 608–612.

118. Hu Z, Zhang A, Storz G, Gottesman S, Leppla SH. An antibody-based microarray assay for small RNA detection. Nucleic Acids Research. 2006;34: e52–e52. doi:10.1093/nar/gkl142

119. Shaw NN, Arya DP. Recognition of the unique structure of DNA:RNA hybrids. Biochimie. 2008;90: 1026–1039. doi:10.1016/j.biochi.2008.04.011

120. Kinney JS, Viscidi RP, Vonderfecht SL, Eiden JJ, Yolken RH. Monoclonal antibody assay for detection of double-stranded RNA and application for detection of group A and non-group A rotaviruses. J Clin Microbiol. American Society for Microbiology (ASM); 1989;27: 6–12.

121. Phillips DD, Garboczi DN, Singh K, Hu Z, Leppla SH, Leysath CE. The sub-nanomolar binding of DNA-RNA hybrids by the single-chain Fv fragment of antibody S9.6. J Mol Recognit. 2013;26: 376–381. doi:10.1002/jmr.2284

122. Ginno PA, Lott PL, Christensen HC, Korf I, Chédin F. R-loop formation is a distinctive characteristic of unmethylated human CpG island promoters. Mol Cell. 2012;45: 814–825. doi:10.1016/j.molcel.2012.01.017

123. Chan YA, Aristizabal MJ, Lu PYT, Luo Z, Hamza A, Kobor MS, et al. Genome-wide profiling of yeast DNA:RNA hybrid prone sites with DRIP-chip. PLoS Genet. Public Library of Science; 2014;10: e1004288. doi:10.1371/journal.pgen.1004288

124. Hage El A, Webb S, Kerr A, Tollervey D. Genome-wide distribution of RNA-DNA hybrids identifies RNase H targets in tRNA genes, retrotransposons and mitochondria. PLoS Genet. 2014;10: e1004716. doi:10.1371/journal.pgen.1004716

125. French S. Consequences of replication fork movement through transcription units in vivo. Science. 1992;258: 1362–1365.

126. Helmrich A, Ballarino M, Nudler E, Tora L. Transcription-replication encounters, consequences and genomic instability. Nat Struct Mol Biol. 2013;20: 412–418. doi:10.1038/nsmb.2543

127. Takeuchi Y, Horiuchi T, Kobayashi T. Transcription-dependent recombination and the role of fork collision in yeast rDNA. Genes & Development. Cold Spring Harbor Lab; 2003;17: 1497–1506. doi:10.1101/gad.1085403

128. Prado F, Aguilera A. Impairment of replication fork progression mediates RNA polII transcription-associated recombination. The EMBO Journal. EMBO Press; 2005;24: 1267–1276. doi:10.1038/sj.emboj.7600602

129. Zeman MK, Cimprich KA. Causes and consequences of replication stress. Nature Cell Biology. 2014;16: 2–9. doi:10.1038/ncb2897

130. Hanada K, Budzowska M, Davies SL, van Drunen E, Onizawa H, Beverloo HB, et al. The structure-specific endonuclease Mus81 contributes to replication restart by generating double-strand DNA breaks. Nat Struct Mol Biol. 2007;14: 1096–1104. doi:10.1038/nsmb1313

131. Lopes M, Foiani M, Sogo JM. Multiple mechanisms control chromosome integrity after replication fork uncoupling and restart at irreparable UV lesions. Mol Cell. 2006;21: 15–27. doi:10.1016/j.molcel.2005.11.015

132. Wimberly H, Shee C, Thornton PC, Sivaramakrishnan P, Rosenberg SM, Hastings PJ. R-loops and nicks initiate DNA breakage and genome instability in non-growing Escherichia coli. Nat Commun. 2013;4: 2115. doi:10.1038/ncomms3115

Chapter II. RNase H enables efficient repair of R-loop induced DNA damage

Introduction

R-loops are structures that form when RNA invades double stranded DNA and hybridizes to complementary genomic sequences [1]. R-loops can form spontaneously across many genomic loci, but the activity of two endogenous RNases H prevents their accumulation and persistence [2]. RNase H1 and H2 are highly conserved ribonucleases with the ability to degrade the RNA moiety of a DNA:RNA hybrid. Disrupting the activity of the two enzymes (*rnh1*Δ *rnh201*Δ in yeast) has been a useful tool for increasing the persistence of DNA:RNA hybrids and studying the effects of hybrid-induced instability. Indeed, efforts to map R-loops genome-wide have shown that in the absence of RNase H activity, the levels of hybrids formed at spontaneous loci increase dramatically [3, 4]. This increase in hybrids is associated with increased rates of genome instability that include loss of heterozygosity (LOH) events, loss of entire chromosomes, and recombination at the ribosomal locus [4,5]. The RNases H have therefore been implicated as important protectors of genome stability.

The ribosomal locus (rDNA) appears to be particularly prone to R-loops. Approximately 60% of all transcription in the cell is devoted to producing ribosomal RNA from about 150 repeated units located in a clustered region on chromosome XII [6]. These repeats, at 9.1 kb each, make up about 10% of the yeast genome. Accordingly, almost 50% of all R-loops map to the rDNA [3]. R-loops found at the rDNA are associated with increased rates of recombination [4,7], RNA polymerase pileups [8], and stalled replication forks [9].

A growing body of evidence has attributed various biological roles to R-loops, including modifying gene expression [10,11], terminating transcription [12,13], driving sequence mutation [14], and inducing changes in genome structure [15,16]. However, the mechanisms of R-loop induced genome instability remain elusive. Most studies on the mechanisms of hybrid-induced instability have been "damage-centric," investigating how R-loops are converted to mutations, single stranded nicks, and double stranded breaks (DSBs) [17]. Current models focus on the involvement of active replication forks that stall or collapse upon encountering the aberrant structure. While this remains an area of active research, we note that any instability event is the result of a complex interplay between the initial damage event and the repair processes that follow. Phenotypes that involve the loss of genetic information (terminal deletions, certain LOH events) imply both that damage occured and that repair processes failed to accurately maintain the genome. Few studies have investigated how R-loop induced damage is repaired, and it remains possible that defects in repair contribute to instability. This possibility raises several questions. First, do genomic changes induced by R-loops reflect increases in

damage events, failures of repair, or both? Second, are specific pathways involved in the repair of R-loop induced damage, and if so, what are they?

To begin to answer these questions, we turned to the Rad52-GFP foci system in yeast. Rad52 is required in almost all homologous recombination pathways, and in yeast forms bright foci upon induction of DNA damage [18]. Most foci appear in the S/G2-M phases of the cell cycle and have a moderate rate of repair – almost all spontaneous Rad52-GFP foci are resolved within 40 minutes [19]. Consistent with phenotypes of increased genomic instability, *rnh1*Δ *rnh201*Δ mutants display an increase in Rad52-GFP foci. A large fraction of these foci appear to co-localize with the nucleolus and form in a window between late S and mid-M [9]. Here, by monitoring the persistence of Rad52 foci across the cell cycle in RNase H mutants, we implicate DNA:RNA hybrids in the disruption of DNA damage repair. We show that topoisomerase I works at the rDNA to prevent these disruptions from becoming lethal events. Furthermore, we identify a new role for the RNases H in preventing break-induced replication (BIR) from repairing R-loop induced DNA damage.

Results

The presence of either RNase H1 or H2 prevents the accumulation of DNA damage in G2-M.

To better understand the mechanisms by which DNA:RNA hybrids contribute to genome instability, we began by characterizing DNA damage in exponentially dividing wild-type, *rnh1*Δ*, rnh201*Δ*,* and *rnh1*Δ *rnh201*Δ budding yeast cells. Using Rad52-GFP foci as a marker for DNA damage, we observed that 27% of *rnh1*Δ *rnh201*Δ cells had foci, a ten-fold increase over wild type, *rnh1*Δ*,* and *rnh201*Δ cells (Figure 1A). Consistent with the notion that persistent DNA damage uniquely affects the double mutants, the growth of the double mutant, but not either of the single mutants, was dramatically impaired by the deletion of *RAD52* (Figure 1B). Previous characterization of the double mutant also reported elevated foci and Rad52-dependent growth [9,20]. Thus, by measures of Rad52-GFP foci and Rad52-dependent growth, cells lacking RNase H1 and H2 have a larger fraction of persistent R-loop induced damage than wild-type cells or cells lacking only one of the RNases H. This persistent damage could have arisen from increased R-loop induced damage and/or an inability to efficiently repair that damage.

To further characterize the DNA damage response in *rnh1*Δ *rnh201*Δ cells, we asked whether this damage accumulated within a specific window of the cell cycle. We arrested *rnh1*Δ *rnh201*Δ cells in G1 using the mating pheromone alpha factor and released them into nocodazole, allowing them to proceed synchronously through the cell cycle until they arrested in mid-M phase at the spindle checkpoint (Figure 1C, Supplemental Figure 1A). During this cell cycle progression, aliquots of cells were removed and fixed to assess Rad52-GFP foci accumulation. Cell cycle stage was determined by measuring DNA content using flow cytometry (Supplemental Figure 1A). The fraction of cells with Rad52-GFP foci remained around 10 to 15 percent through S-phase. Additional foci appeared at the S/G2-M boundary and accumulated to around 50 percent, as reported previously. The failure to observe accumulating foci early in the cell

cycle was not a limitation of the system, as an identical analysis of a single cell cycle of *sin3*Δ cells, which also accumulate hybrids, revealed an increase in focus formation during S-phase (Supplemental Figure 2A, 2B). The increase in foci in *rnh1*Δ *rnh201*Δ cells did not appear to be due to a cell-cycle dependent increase in hybrid formation, as cytological staining revealed similar levels of R-loops in cells staged in G1, S and M (Figure 1D). Therefore, the increase in damage during the S/G2-M window in *rnh1*Δ *rnh201*Δ cells is likely because hybrids were either more efficiently converted to damage or the repair of hybrid-induced damage became impaired.

The presence of DNA damage such as DSBs leads to a Rad9-dependent cell-cycle checkpoint that delays entry into anaphase [21]. We found that the fraction of cycling cells in G2-M, defined as a large-budded morphology with an undivided nucleus, was two-fold higher in *rnh1*Δ *rnh201*Δ cells than wild type or either RNase H single mutant. This fraction was reduced by deletion of *RAD9* (Figure 2A). Deletion of *RAD9* did not decrease the level of Rad52-GFP foci in *rnh1*Δ *rnh201*Δ cells, indicating that focus formation is not dependent on the checkpoint (Figure 1A). To assess the kinetics of foci persistence in *rnh1*Δ *rnh201*Δ cells, we arrested cultures in S-phase using hydroxyurea and released them into alpha factor, allowing them to proceed through M-phase and arrest in the following G1 (Figure 2B and Supplemental Figure 1B). After the expected increase of Rad52-GFP foci upon the completion of S-phase, we observed a gradual disappearance of foci. Throughout the time-course, the vast majority of cells that retained foci were arrested pre-anaphase, indicating that most cells delayed progression into anaphase until the damage was repaired (Figure 2B). For example, after 330 minutes, the bulk of cells had reached G1 (Figure 2C) and the fraction of cells with Rad52-GFP foci had dropped to 20 percent. Of the cells that retained foci, 77 percent remained arrested in G2-M before anaphase. The slow disappearance of foci and progression into anaphase raised the possibility that hybrid-induced damage might be difficult to repair in a subset of the double mutant cells.

Depletion of topoisomerase-1 exacerbates DNA damage phenotypes in the absence of the RNases H

To improve our ability to interrogate the unusual DNA damage in *rnh1*Δ *rnh201*Δ cells, we sought to strengthen the damage phenotype. A number of observations suggested that alleles of *TOP1*, which encodes the major topoisomerase I in yeast, might be good candidates for doing so. Top1 is thought to clear R-loops and stalled RNA polymerase I (RNA pol I) complexes at the ribosomal locus by resolving supercoiling [8,22,23]. A potential synergistic relationship between Top1 and the RNases H came from the observation that while cells with either the *top1*Δ mutation or the *rnh1*Δ *rnh201*Δ mutations are viable, the *top1*Δ *rnh1*Δ *rnh201*Δ mutant is inviable [8]. Furthermore, treatment of *rnh1*Δ *rnh201*Δ cells with the Top1 inhibitor camptothecin led to increased Rad52-GFP foci that co-localized with the nucleolus [9]. Encouraged by these results, we used the auxin-inducible degron (AID) system to create a conditional *TOP1-AID* allele in wild type, the two single RNase H mutants, and the double RNase H mutant. We then reassessed viability and DNA damage phenotypes.

Consistent with published results, *rnh1*Δ *rnh201*Δ *TOP1-AID* cells fail to grow when treated with auxin (Figure 3A). In contrast, *TOP1-AID*, *rnh1*Δ *TOP1-AID*, and

*rnh201*Δ *TOP1-AID* mutants grew well. Thus, the synergistic lethality occurred only when both RNases H and Top1 were inactivated. Similarly, when exponential cultures of these strains were treated with auxin for four hours, Rad52-GFP foci did not increase in *TOP1-AID*, *rnh1*Δ *TOP1-AID* or *rnh201*Δ *TOP1-AID* mutants (Figure 3B). However, foci nearly doubled in the *rnh1*Δ *rnh201*Δ *TOP1-AID* cells compared to an untreated control, such that a large majority of *rnh1*Δ *rnh201*Δ *TOP1-AID* cells (85%) had foci. Furthermore, after four hours of treatment with auxin, over 98 percent of *rnh1*Δ *rnh201*Δ *TOP1-AID* cells were arrested pre-anaphase at the G2-M checkpoint (Figures 3C and 3D). This arrest reflected an exacerbation of the cell cycle delay observed in the *rnh1*Δ *rnh201*Δ strain and in *rnh1*Δ *rnh201*Δ *TOP1-AID* cells left untreated with auxin (Figures 2A and 3C). As with *rnh1Δ rnh201Δ* cells, the cell-cycle arrest of the *rnh1*Δ *rnh201*Δ *TOP1-AID* was Rad9 dependent; deletion of *RAD9* resulted in cells that proceeded into the following G1. Importantly, deletion of *RAD9* did not restore viability to *rnh1*Δ *rnh201*Δ *TOP1-AID* cells treated with auxin. This result suggests that the inviability of the triple mutant was not simply due to the constitutive activation of the checkpoint but rather to the presence of irreparable damage.

A striking feature of the Rad52-GFP foci in the *rnh1*Δ *rnh201*Δ double mutant was that they accumulated in a window that began at the boundary between S and G2-M. Therefore, we tested whether the enhanced focus formation in the *rnh1*Δ *rnh201*Δ *TOP1-AID* cells also occurred in this window (Figure 4A). A culture of the *rnh1*Δ *rnh201*Δ *TOP1-AID* triple mutant was arrested in G1 with alpha factor and treated with auxin to deplete Top1-AID (Supplemental Figures 3A and 3C). Cells were released from G1 into media containing auxin and nocodazole, to perpetuate Top1-AID depletion and induce subsequent arrest in mid-M (Supplemental Figure 3A). Aliquots were removed as cells progressed from G1 to mid-M arrest and assessed for Rad52-GFP foci. As a control, a second culture was subjected to the same regime without auxin.

The enhanced foci in the triple mutant exhibited the same kinetics of accumulation as the double mutant (Figure 4A). The fraction of triple mutant cells with Rad52-GFP foci in both cultures remained around 15 to 20 percent until the end of bulk S-phase, similar to the *rnh1*Δ *rnh201*Δ double mutant. At subsequent time points, the auxin-free triple mutant culture mimicked the double mutant, as foci rose to about 45 percent in G2-M. The fraction of Rad52-GFP foci in the triple mutant cells treated with auxin also rose in G2-M but to a higher value of about 75 percent. Taken together, the triple mutant exhibited qualitatively similar but quantitatively greater cell cycle and DNA damage defects relative to the double mutant, indicating that Top1 depletion enhanced the DNA damage phenotype caused by loss of RNase H activity.

The ability to conditionally inactivate Top1-AID allowed us to address the role of Top1 activity in the cell-cycle dependent appearance of Rad52-GFP foci and the connection between focus formation and lethality. Cultures of *rnh1*Δ *rnh201*Δ *TOP1-AID* cells were arrested in mid-M with nocodazole and then treated with auxin. Top1-AID was depleted within 30 minutes of addition of auxin (Supplemental Figures 3B and 3C). The fraction of cells with Rad52-GFP foci climbed to about 70 percent (Figure 4B). This result suggested that Top1 activity was required after the completion of bulk S-phase to prevent focus formation.

To address whether Rad52-GFP foci induced by Top1 depletion were correlated with lethality, asynchronously dividing *rnh1*Δ *rnh201*Δ *TOP1-AID* cells were transiently treated with auxin for four hours, washed with fresh media, and then plated onto nonselective plates. The fraction of cells that survived, relative to an untreated control, was around 16 percent, similar to the percentage of cells that did not have Rad52 foci when given the same treatment (Figure 4C). This correlation suggested that the persistent foci in the *rnh1*Δ *rnh201*Δ *TOP1-AID* cells represented lethal DNA damage that arose from inactivation of Top1 activity in G2-M. To test this hypothesis further, we asked whether the appearance of foci was temporally correlated with inviability. The *rnh1*Δ *rnh201*Δ *TOP1-AID* cells were first arrested in S- or mid-M phase with hydroxyurea or nocodazole, respectively. The arrested cells were treated with auxin to deplete Top1-AID activity. These cells were plated for viability on media lacking auxin, allowing the restoration of Top1-AID activity (Figure 4C). Transiently depleting Top1 in S-phase, in which foci levels remain unchanged (18%), did not lead to loss of viability. However, transiently depleting Top1 in mid-M phase, which led to elevated foci levels (75%), also led to a dramatic increase in lethality. These results suggest that depletion of Top1 activity in G2-M in cells lacking the RNases H leads to irreparable DNA damage in the vast majority of cells.

PIF1-E467G enables repair of R-loop mediated DNA damage

The lethality of *rnh1*Δ *rnh201*Δ cells upon Top1 inactivation provided a powerful genetic tool to interrogate R-loop induced DNA damage. Suppressor mutations that allowed a strain lacking both RNases H and Top1 to survive could either prevent damage from occurring or allow that damage to become reparable. These suppressor mutations could inform us about the processes that convert R-loops to DNA damage or the mechanisms by which R-loop mediated damage is repaired. To isolate these suppressors, we generated independent cultures of an *rnh1*Δ *rnh201*Δ *top1*Δ strain that contained a plasmid carrying the *RNH1* and *URA3* genes. Plating these cultures on 5-fluoroorotic acid (5-FOA) selected for cells that had lost the plasmid and thus carried a suppressor mutation that allowed them to divide despite their *rnh1*Δ *rnh201*Δ *top1*Δ genotype (Figure 5A).

DNA sequencing of the suppressor strains identified *PIF1-E467G*. E467G is a novel mutation in Pif1, a helicase with multiple roles in nuclear and mitochondrial DNA metabolism. This allele suppressed auxin sensitivity when introduced into *rnh1*Δ *rnh201*Δ *TOP1-AID* cells, indicating its responsibility for the suppression of lethality in *rnh1*Δ *rnh201*Δ *top1*Δ cells (Figure 5B). This allele was not found in any previously described domains of Pif1 (Figure 5A), prompting us to assess the ability of well-characterized recessive *PIF1* alleles to suppress the lethality of *rnh1*Δ *rnh201*Δ *top1*Δ genotype [24]. When introduced into *rnh1*Δ *rnh201*Δ *TOP1-AID*, both *pif1*Δ and *pif1-m2*, an allele that maintains mitochondrial but not nuclear functions of Pif1 [25], were able to suppress the auxin sensitivity of *rnh1*Δ *rnh201*Δ *TOP1-AID* cells. We conclude that *PIF1-E467G* likely inactivates a nuclear activity that is contributing to hybrid-induced lethality.

To determine whether *PIF1-E467G* prevented hybrid-induced DNA damage in *rnh1*Δ *rnh201*Δ *TOP1-AID* cells or allowed for its repair, we monitored the appearance

and disappearance of Rad52-GFP foci in synchronously dividing cells. A culture of *rnh1*Δ *rnh201*Δ *TOP1-AID PIF1-E467G* cells was arrested in G1 (alpha factor) and treated with auxin to deplete Top1-AID. The culture was switched into media containing nocodazole and auxin to perpetuate Top1-AID depletion and allow progression through the cell cycle until arrest in mid-M phase (Figure 5C, Supplemental Figure 4A). The pattern of appearance of Rad52-GFP foci in this culture showed a strong similarity to the parent strain expressing wild-type Pif1, with no increase in foci until the completion of bulk S-phase. The fraction of cells containing Rad52-GFP foci then rose to 80 percent with auxin treatment and 40 percent without. These results suggest that the *PIF1-E467G* allele does not prevent hybrid induced DNA damage.

We next compared the appearance and disappearance of Rad52-GFP foci in *rnh1*Δ *rnh201*Δ *TOP1-AID* and *rnh1*Δ *rnh201*Δ *TOP1-AID PIF1-E467G* strains as they progressed between S phase to the subsequent G1. Cultures of these cells were arrested in hydroxyurea to induce S-phase arrest and then treated with auxin to induce Top1-AID depletion. The cultures were switched into media with auxin and alpha factor to perpetuate Top1-AID depletion and allow progression through mitosis to the next G1 (Figure 5B, Supplemental Figure 4B). In contrast to *rnh1*Δ *rnh201*Δ *TOP1-AID* cells, which maintained 85% Rad52-GFP foci and never proceeded through anaphase, cells with *PIF1-E467G* gradually resolved most of their foci as they completed mitosis. We therefore conclude that *PIF1-E467G* promotes the repair of hybrid-induced damage.

Novel alleles of RNA polymerase I enable repair of R-loop mediated DNA damage

Our genetic screen also identified *RPA190-K1482T and RPA190-V1486F,* two novel alleles of Rpa190, the largest subunit of RNA pol I (Figure 6A). These residues map to the "jaw" domain of the RNA Pol I complex [26,27]. They are distinct from a previously tested Rpa190 allele that has been shown to suppress *rnh1*Δ *rnh201*Δ *top1*Δ inviability (*rpa190-3)*, and which is found closer to the dNTP entry pore of the polymerase [9,28]. *RPA190-K1482T* and *RPA190-V1486F* share the suppression phenotypes of *PIF1-E467G*. Both *RPA190* alleles suppress the auxin-induced inviability of *rnh1*Δ *rnh201*Δ *TOP1-AID* cells (Figure 6A). Similarly, neither allele prevents the accumulation of high levels of foci, but rather allow for their repair (Figures 6C and 6D, Supplemental Figures 5A and 5B). Given the specificity of RNA Pol I for transcribing regions of the rDNA locus, these results strongly suggest that the lethality in *rnh1*Δ *rnh201*Δ *top1*Δ is due to irreparable hybrid-induced DNA damage in the ribosomal repeats on chromosome XII and that altering the function of RNA polymerase I can allow this damage to be repaired.

To begin to understand the mechanism by which these alleles modify the activity of RNA pol I, we turned to previously reported crystal structures of the RNA pol I complex. Residues K1482 and V1486 in Rpa190 are found along potential contacts with the non-essential RNA pol I subunit Rpa12 (Supplemental Figures 6A-6C). Rpa12 has a role in promoting RNA Pol I backtracking and transcript termination [29,30]. This backtracking activity may affect genome stability – recent studies in bacteria have shown that backtracked RNA polymerases can cause R-loop dependent DSBs due to co-directional collisions with replisomes [31]. The proximity of Rpa12 to our suppressor mutations suggested that Rpa12 activities might be important for repair of the hybrid-

induced damage. To test this idea, we knocked out Rpa12 in *rnh1*Δ *rnh201*Δ *top1*Δ *RPA190-K1482T* cells (Figure 6B). Deleting Rpa12 in these cells was lethal, indicating that our new *RPA190* alleles depend upon Rpa12, and by inference, polymerase backtracking or termination to repress hybrid-induced lethality.

Break induced replication is responsible for inability to repair damage

Taken together, our studies implicate Pif1, RNA pol I and the rDNA locus, and a G2-M specific process in the cell's inability to repair hybrid-induced damage. These observations led us to question the role of break-induced replication (BIR) in hybrid-mediated instability. BIR is an HR-dependent repair process that occurs in G2-M when only one end of a DSB is available for recombination [32]. This end can be captured by homologous sequences and used as a primer for replication [33]. Break-induced replication is extremely processive and can extend the length of entire chromosomes, in part due to the contribution of the Pif1 helicase [34,35].

First, we asked how the *PIF1-E467G* allele functions in BIR. To do this, we introduced the allele into a previously characterized *in vivo* system for assessing BIR [36]. Briefly, these strains carry an inducible HO endonuclease cut site centromere-distal to an incomplete *URA3* gene on chromosome V. Upon induction of a DSB, a telomere needs to be added to the chromosome to restore viability to the cell. This repair can proceed with BIR using homology from an incomplete *URA3* repair template on the opposite arm. The repair template is situated in a position that requires either 30 or 80 kb of BIR for telomere addition, the latter being less efficient. Repair by BIR results in a fully functional *URA3* gene, thereby conferring the ability to grow on media lacking uracil.

In a wild-type strain, the frequency of BIR using the 30kb template is approximately 12%, consistent with previously published results (Figure 7A). In the absence of a functional Pif1 allele (*pif1-m2)*, repair by BIR drops to approximately 5%. Similarly, the frequency of BIR in cells carrying *PIF1-E467G* dropped to around 3%. In the 80kb repair template strain, a similar pattern in BIR efficiency was seen (Figure 7B). Strains carrying the *pif1-m2* or *PIF1-E467G* alleles saw drops in BIR frequency from approximately 5% to 1%. This led us to conclude that *PIF1-E467G* inhibits BIR. We observed no change in repair events in *top1*Δ cells, indicating that the absence of Top1 does not interfere with BIR.

The common phenotype for *PIF-E467G* and *pif1-m2* was inhibition of BIR, suggesting that this inhibition was responsible for allowing repair of the otherwise lethal hybrid-induced DNA damage. To test this model further, we deleted *POL32* in *rnh1*Δ *rnh201*Δ *TOP1-AID* cells (Figure 5B). Pol32 is a non-essential subunit of the primary BIR polymerase (Polδ), and is required for replication fork processivity [35]. These strains were no longer sensitive to auxin, corroborating the conclusion that inhibiting BIR is sufficient to allow for repair of otherwise lethal hybrid-induced DNA damage. Taken together, these results suggest that the attempt to repair hybrid-induced damage in the rDNA by BIR leads to an irreparable state.

PIF1-E467G promotes an alternative pathway for repair. In wild-type cells, almost all repair events after DSB induction used BIR. In contrast, *PIF1-E467G* cells had a near wild-type level of viability after DSB induction but used BIR only 20 percent of

the time (Figures 7A and 7B). Thus, BIR was compromised, but an alternative pathway stepped in to promote telomere addition. As expected if this repair was independent of BIR, this alternative pathway was as efficient with the 80kb repair template as it was in cells with the 30 kb repair template; *PIF1-E467G* cells in the 80 kb repair strain had a total level of repair that was 5-fold greater than wild-type cells but only six percent of which was repaired using BIR. This alternative pathway was poorly activated in *pif1-m2* cells, as evidenced by a depressed level of viability. The increase in repair was not due to increased non-homologous end joining, as less than one percent of cells of all genotypes retained a telomeric drug resistance marker (Supplemental Figures 7A and 7B). Additionally, all strains efficiently induced DSBs, since PCR primers surrounding the cut site failed to amplify DNA after HO induction (Supplemental Figure 7C). Further analyses will be necessary to identify the alternative pathway for repair of hybrid-induced damage.

Discussion

Our observations in this study suggest that the absence of the two RNases H leads to DNA damage that is difficult to repair after completion of S-phase. First, we observe an increase in Rad52 foci only in cells lacking both RNases H (*rnh1*Δ *rnh201*Δ). The increase in foci begins at the exit from S-phase and continues until mid-M. We show that this damage induces a significant pre-anaphase delay by activating the Rad9-dependent checkpoint. When measured in a bulk population, foci disappear slowly such that even after most cells have lost foci and completed cell division, a subset of cells retain foci and remain arrested pre-anaphase. This phenotype is indicative of an inability to efficiently repair damage. The depletion of Top1 in *rnh1*Δ *rnh201*Δ cells appears to exacerbate this problem by generating more foci that lead to lethal, irreparable damage and permanent arrest. Importantly, disrupting factors that modulate BIR allows for repair of these foci and restores cell division without reducing the initial level of damage. This demonstrates that the inability to repair damage, not the level of damage *per se*, in *rnh1*Δ *rnh201*Δ cells is the root cause of the inability to proceed through the cell cycle. Taken together, these results suggest that DNA:RNA hybrids inhibit DNA repair and that a critical role of the RNases H is to remove hybrids so that efficient repair can occur.

While hybrids have been recognized for many years as agents of genome instability, most studies have focused on their ability to generate DNA damage rather than their ability to alter DNA repair. However, a number of observations support our hypothesis of R-loops as inhibitors of repair. Inactivation of RNase H2 (*rnh201*Δ) by itself leads to large increases of genomic hybrids and loss of heterozygosity compared to wild-type [3,5]. This result suggests that loss of RNase H2 generates elevated levels of DNA damage. However, dramatically elevated Rad52 foci are only observed in *rnh1*Δ *rnh201*Δ cells – not *rnh201*Δ cells. We suggest that damage may be repaired rapidly in cells lacking RNase H2, while damage is repaired slowly in cells lacking both RNases H, causing foci to accumulate and persist.

Additionally, *sin3*Δ cells have elevated R-loops and hybrid-mediated genome instability. Inactivation of RNase H1 in *sin3*Δ cells increases genome instability further,

but skews the events from chromosome repair to chromosome loss [4]. This result also supports a role for RNase H1 as critical in allowing repair of hybrid-induced damage. Presumably, under conditions of elevated hybrid formation such as *sin3*Δ, inactivation of RNase H1 alone is sufficient to cause a repair problem.

An insight into a potential role for the RNases H in DNA repair comes from a key observation in this study: lethality in *rnh1*Δ *rnh201*Δ cells when they are depleted of Top1 can be suppressed by mutations in Pif1 or Pol32 that inhibit BIR. The severity of the lethality – 88% cell death in a single cell cycle – suggests that BIR is a major pathway for the repair of R-loop induced damage in RNase H deficient cells. Consistent with this conclusion, previous studies mapped recombination events genome-wide in RNase H single and double mutants and found that 50% of the repair events occurred through BIR [5]. Furthermore, the percent of repair by BIR was elevated about 5 fold in the double mutant compared to either of the singles or wild type, although validation of this difference awaits a larger sample size.

To explain the BIR bias, we suggest that the RNases H remove hybrids from chromosomes both before and after R-loops induce DSBs (Figure 8A). Conversely, in the absence of RNase H activity, more DSBs are induced and hybrids persist at these DSBs. While one free end of the DSB may be properly processed by HR machinery, the presence of a hybrid on the opposite free end may block resection and/or invasion of homologous sequences. Ultimately, failure to capture the second free end of the DSB leads to BIR.

Why does hybrid-induced BIR lead to cell-cycle arrest and a complete abrogation of repair when Top1 is depleted? An important clue comes from the fact that the lethality of *rnh1*Δ *rnh201*Δ *top1*Δ cells can be suppressed by mutations in RNA pol I, an enzyme whose function is limited to transcribing ribosomal DNA. The rDNA is the biggest source of R-loops in cells, accounting for almost 50% of all hybrids in yeast [3]. These results suggest that BIR at the rDNA may be particularly challenging in the presence of hybrids and even more challenging in the absence of Top1. We therefore propose that the induction of hybrids in the rDNA generates a barrier to the processivity of DNA replication during BIR, thereby slowing repair (Figure 8B). Further inactivation of Top1 causes elevated hybrids and stalled polymerases, which we hypothesize terminally block BIR replication fork progression. This trapped BIR intermediate is an aberrant structure that then leads to lethality. Interestingly, stalled replication forks have been observed at the rDNA locus in *rnh1*Δ *rnh201*Δ cells depleted of Top1 [9]. While these forks have been interpreted as being induced by aberrant DNA replication priming by the RNA moiety of R-loops, they equally well could have arisen from stalled BIR intermediates.

The mutations in RNA pol I that suppress the lethality of *rnh1*Δ *rnh201*Δ *top1*Δ map to the interface between subunits Rpa190 and Rpa12. This suppression is dependent upon Rpa12, a factor known to alleviate stalled polymerases either by promoting backtracking or transcription termination. Stalled RNA polymerases have been linked to R-loop dependent replication fork collisions that cause DSBs [31]. We therefore suggest that the *RPA190* suppressor mutations activate Rpa12, allowing it to remove stalled polymerases and possibly the associated hybrids, thereby removing the impediment to BIR imposed by Top1 (Figure 8B).

Our model for stalled BIR intermediates as the cause of lethality in *rnh1*Δ *rnh201*Δ *top1*Δ cells is supported by the molecular functions of Pif1 and Pol32. BIR is known to be a multi-step process in which strand invasion happens rapidly followed by a long delay before replication initiates [37]. This delay would explain the slow disappearance of hybrid-induced Rad52-GFP foci in *rnh1*Δ *rnh201*Δ cells. After this pause, Pif1 and Pol32 are required for processivity of the BIR replication fork. We suggest that inhibition of these two factors causes the invading strand to dissociate before it can reach the blocks imposed by the hybrids and/or RNA polymerases. A slower, alternative pathway, the identity of which remains unclear, can then repair the released strand.

In summary, we show that the RNases H play a critical role in promoting proper repair of hybrid-induced DNA damage, particularly in highly transcribed repetitive DNA. This conclusion came from directly limiting RNase H activity in cells and observing hybrid-induced BIR. Other conditions may also effectively limit RNase H activity. For example, many RNA biogenesis mutants induce hybrid formation and elevate genome instability [4]. The genome instability of these mutants can be suppressed by overexpression of RNase H, implying that RNase H activity becomes limiting when hybrid levels exceed a threshold. It has been assumed that this instability results only from increased damage induced by the persistence of R-loops. However, in light of our results, it is likely that limiting RNase H activity in these mutants also allows hybrids to promote BIR-induced genome instability. Finally, the particular sensitivity of the highly transcribed rDNA repeats is intriguing given that many cancer cells contain highly transcribed amplicons. These amplicons may be not only sites of R-loop formation and R-loop induced DNA damage, but also sites of improper repair.

Figures

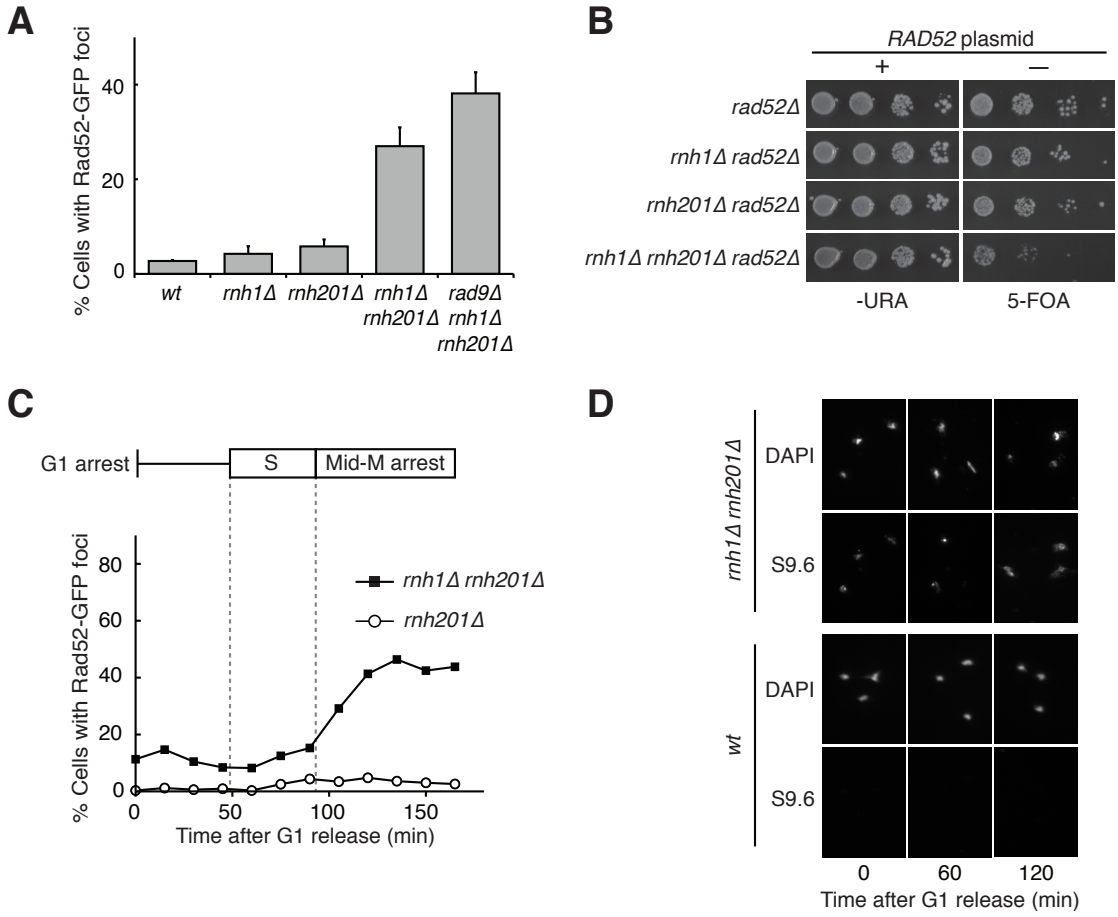

Figure 1 – *Cells lacking both RNases H accumulate DNA damage in G2-M.* (A) Assessment of Rad52-GFP in RNase H mutants. Asynchronously dividing cells were scored for the presence of one or more Rad52-GFP focus. Bars represent mean +/- standard deviation (*n=3*; 300 cells scored per replicate). (B) Assessment of Rad52 requirement in RNase H mutants. Cells carrying a plasmid expressing *RAD52* and *URA3* were plated onto media lacking uracil (-URA, selects for plasmid) or media containing 5-floroorotic acid (5-FOA, selects for plasmid loss). 10-fold serial dilutions are shown. (C) Cell cycle profile of Rad52-GFP foci in RNase H mutants. Synchronously dividing cells were scored for the presence of Rad52-GFP foci. Cells arrested in G1 using alpha factor were washed and released into nocodazole. Samples were taken at 15-minute intervals and 300 cells per time point were scored for Rad52-GFP foci. Cell cycle phase is determined by flow cytometry (Supplemental Figure 2A). (D) Cell cycle profile of DNA:RNA hybrids in RNase H mutants. Shown are representative images of chromosome spreads of *rnh1*Δ *rnh201*Δ and *wild-type* cells. Spreads are stained for DNA content (DAPI) or immunostained for DNA:RNA hybrids using the S9.6 antibody and a fluorescent-conjugated secondary.

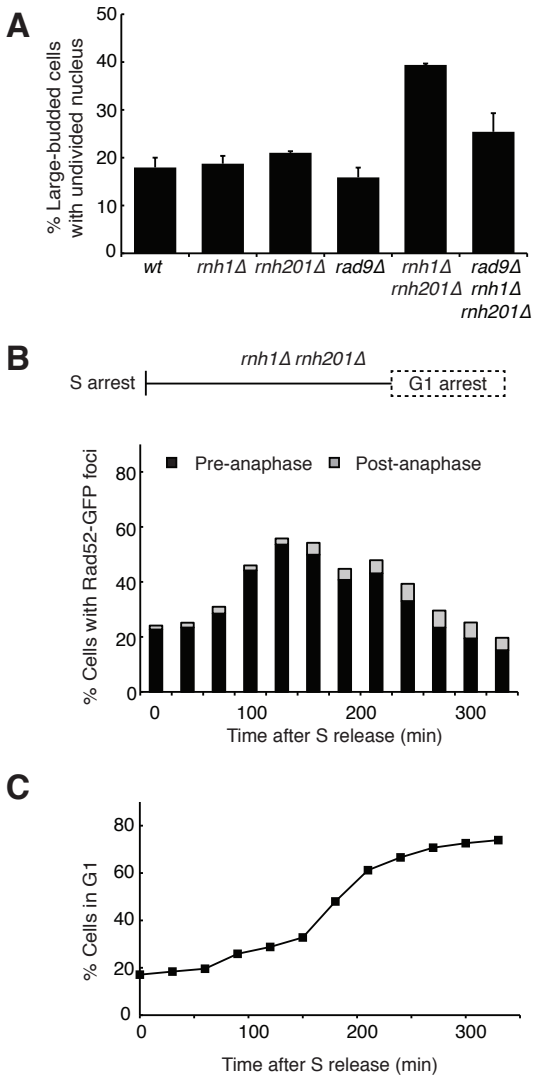

Figure 2 – *Cells with hybrid-induced DNA damage are slow to repair.* (A) Assessment of cell-cycle delay in RNase H mutants. Asynchronously dividing cells were scored on the basis of their bud size and nuclear morphology. The percentage of cells with large buds and an undivided nucleus (single DAPI mass) are shown. Bars represent mean +/- standard deviation (*n=3*, 100 cells scored per replicate) (B) Cell cycle profile of Rad52-GFP foci in dividing cells. *rnh1*Δ *rnh201*Δ cells were arrested in S-phase using hydroxyurea, washed, and released into alpha factor. Samples were taken at 30-minute intervals and 300 cells per time point were scored for Rad52-GFP foci. If a cell had a Rad52-GFP focus, it was further scored for cell cycle phase. Cells with undivided nuclei (single DAPI mass) are labeled "pre-anaphase," while those that had undergone nuclear division (two DAPI masses or G1 arrested) are labeled "post anaphase." (C) Cell cycle stage of dividing *rnh1*Δ *rnh201*Δ cells. Cells from (B) were subjected to flow cytometry (Supplemental Figure 2c) and quantified. The percentage of cells with 1C DNA content is shown.

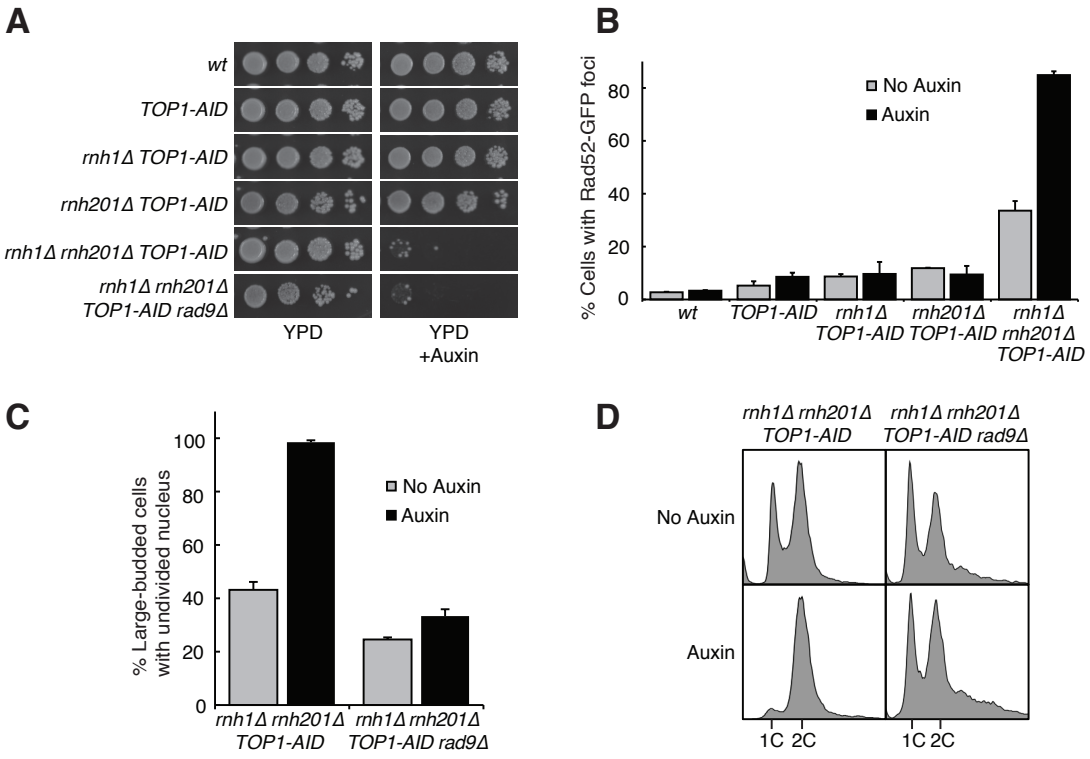

Figure 3 – *Depleting topoisomerase I exacerbates rnh1Δ rnh201Δ phenotypes*. (A) Assessment of Top1 depletion on viability of RNase H mutants. 10-fold serial dilutions of saturated cultures were plated onto rich media (YPD) or media containing auxin (YPD +Auxin). (B) Assessment of Top1 depletion on Rad52-GFP foci in RNase H mutants. Cultures were grown at 23 degrees and treated with auxin for four hours. Cells were then scored for presence of Rad52-GFP foci. Bars represent mean +/- standard deviation (*n=3*, 300 cells scored per replicate). (C) Depleting Top1 leads to robust Rad9-dependent cell cycle arrest. Logarithmically dividing cells were treated with auxin for four hours then scored for bud size and nuclear morphology. The percentage of cells with large buds and undivided nuclei (single DAPI mass) is shown. Bars represent mean +/- standard deviation (*n=3*, 100 cells scored per replicate). (D) Cells from (C) were subjected to flow cytometry.

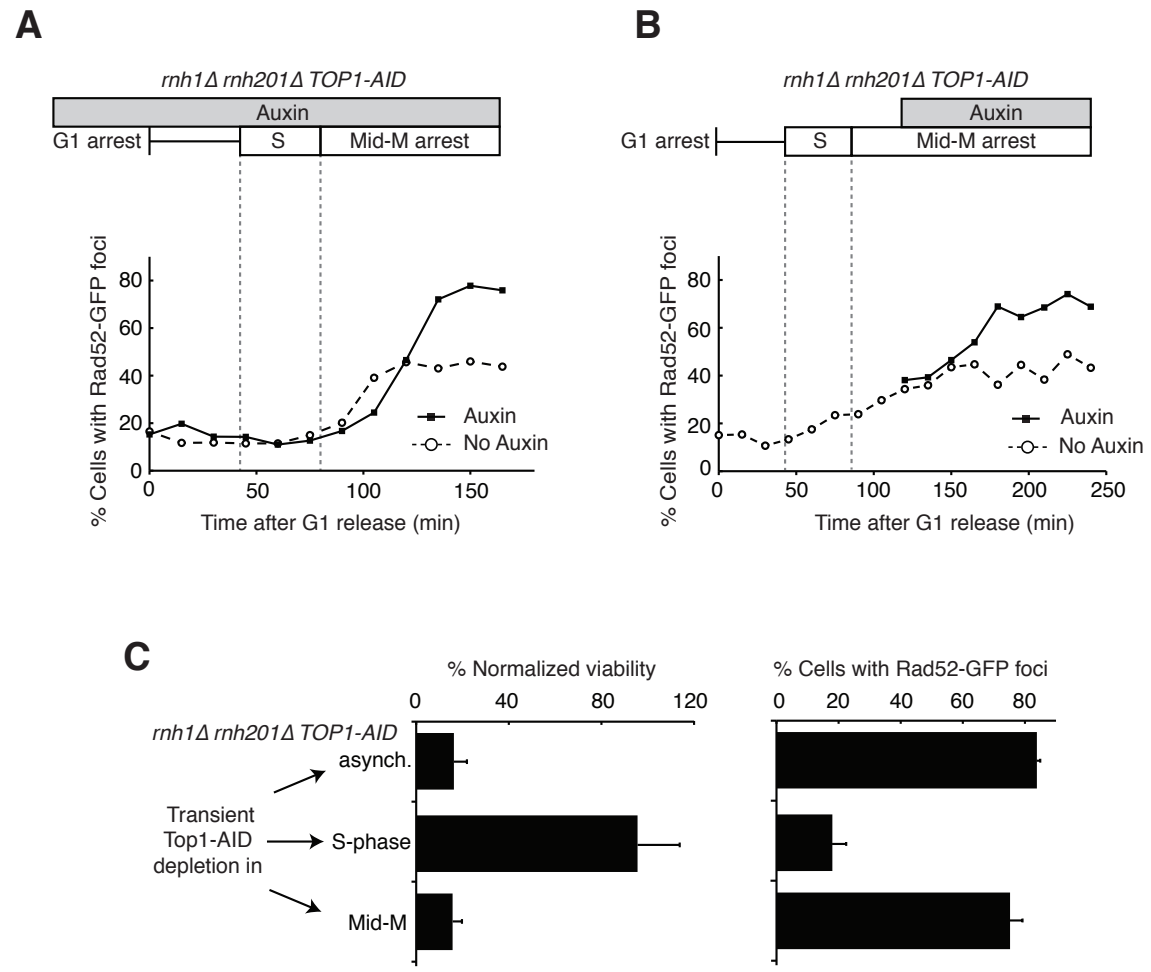

Figure 4 – *Depleting topoisomerase I causes lethal DNA damage in G2-M.* (A) Depleting Top1 in *rnh1*Δ *rnh201*Δ cells shows similar onset of Rad52-GFP at the S/G2-M border. Cultures of *rnh1*Δ *rnh201*Δ *TOP1-AID* cells were arrested in G1 using alpha factor, treated with auxin for 2 hours, then released into media containing nocodazole and auxin. Samples were taken at 15-minute intervals and 300 cells per time point were scored for Rad52-GFP foci. (B) Depleting Top1 in *rnh1*Δ *rnh201*Δ cells after completion of S-phase causes accumulation of Rad52-GFP foci. Cultures of *rnh1*Δ *rnh201*Δ *TOP1-AID* cells were released from alpha factor into nocodazole. Once cells had completed S-phase, auxin was added. Samples were taken at 30-minute intervals and 300 cells per time point were scored for Rad52-GFP foci. (C) Cultures of *rnh1*Δ *rnh201*Δ *TOP1-AID* cells were allowed to divide asynchronously, arrested in S-phase using hydroxyurea, or arrested in Mid-M phase using nocodazole. Once cells were arrested, auxin was added for four hours. *Left* – Cells were then washed and plated on YPD for recovery. Viability was measured by normalizing colony-forming units from auxin-treated cells to untreated cells. Bars represent mean +/- standard deviation (*n=4*). *Right* – Cells are scored for Rad52-GFP foci. Bars represent mean +/- standard deviation (*n=3*, 300 cells scored per replicate).

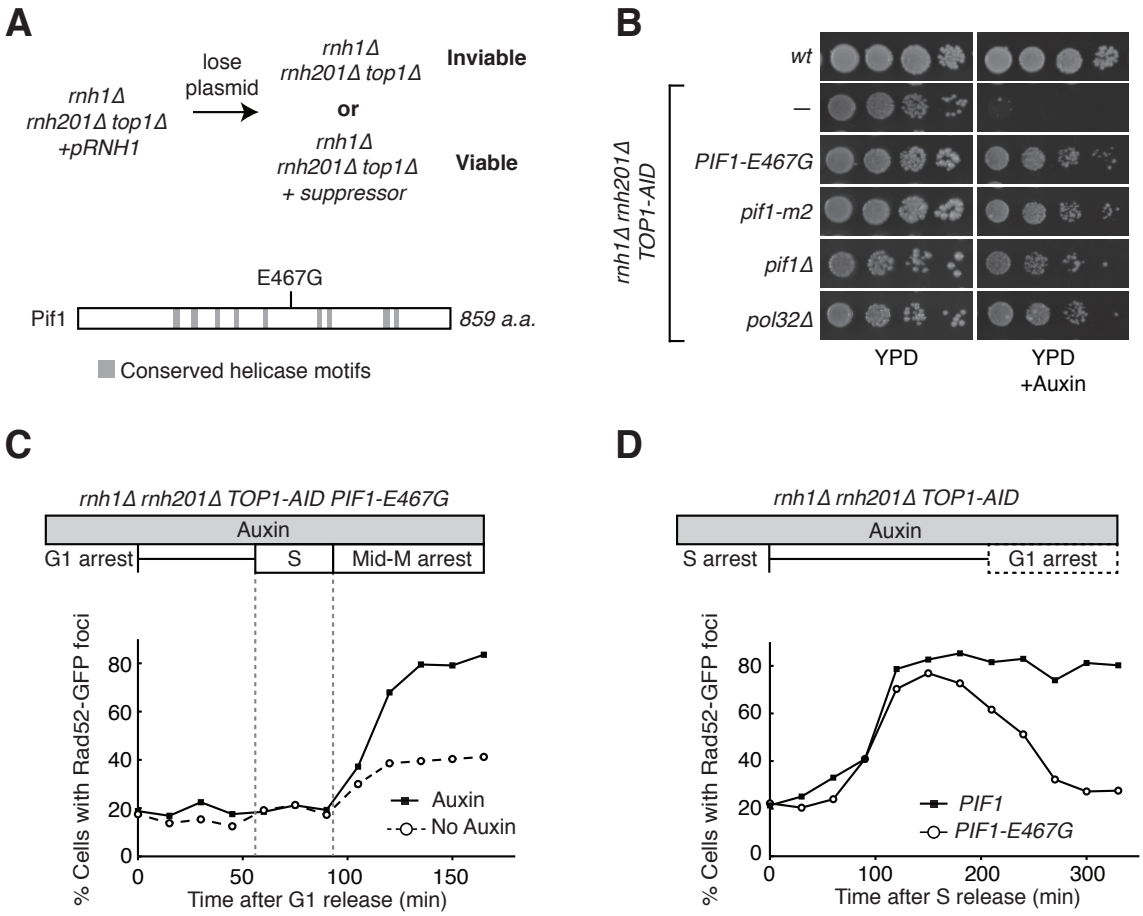

Figure 5 – *Pif1-E467G allows for repair of R-loop induced damage.* (A) *Top*: schematic of genetic screen for suppressors of hybrid-induced lethality. Cells for the screen were *rnh1*Δ *rnh201*Δ *top1*Δ and carried a plasmid expressing *RNH1* and *URA3.* Cultures were grown in non-selective media and plated onto 5-FOA to select for cells that had lost the plasmid and therefore gained suppressor mutations of *rnh1*Δ *rnh201*Δ *top1*Δ lethality. *Bottom:* schematic of Pif1 showing location of E467 relative to evolutionarily conserved SFI helicase motifs and motifs conserved between Pif1 and RecD, as previously published [24]. (B) Mutations in *PIF1* and *POL32* suppress auxin sensitivity of *rnh1*Δ *rnh201*Δ *TOP1-AID* cells. 10-fold serial dilutions of saturated cultures were plated onto YPD or YPD with auxin. (C) Pif1-E467G does not change accumulation of Rad52-GFP foci. Experiment in Figure 4A was repeated on *rnh1*Δ *rnh201*Δ *TOP1-AID PIF1-E467G* cells. (D) Pif1-E467G allows for repair of Rad52-GFP foci. Experiment in Figure 2B was repeated on *rnh1*Δ *rnh201*Δ *TOP1-AID* cells in the presence of auxin with or without *PIF1-E467G.*

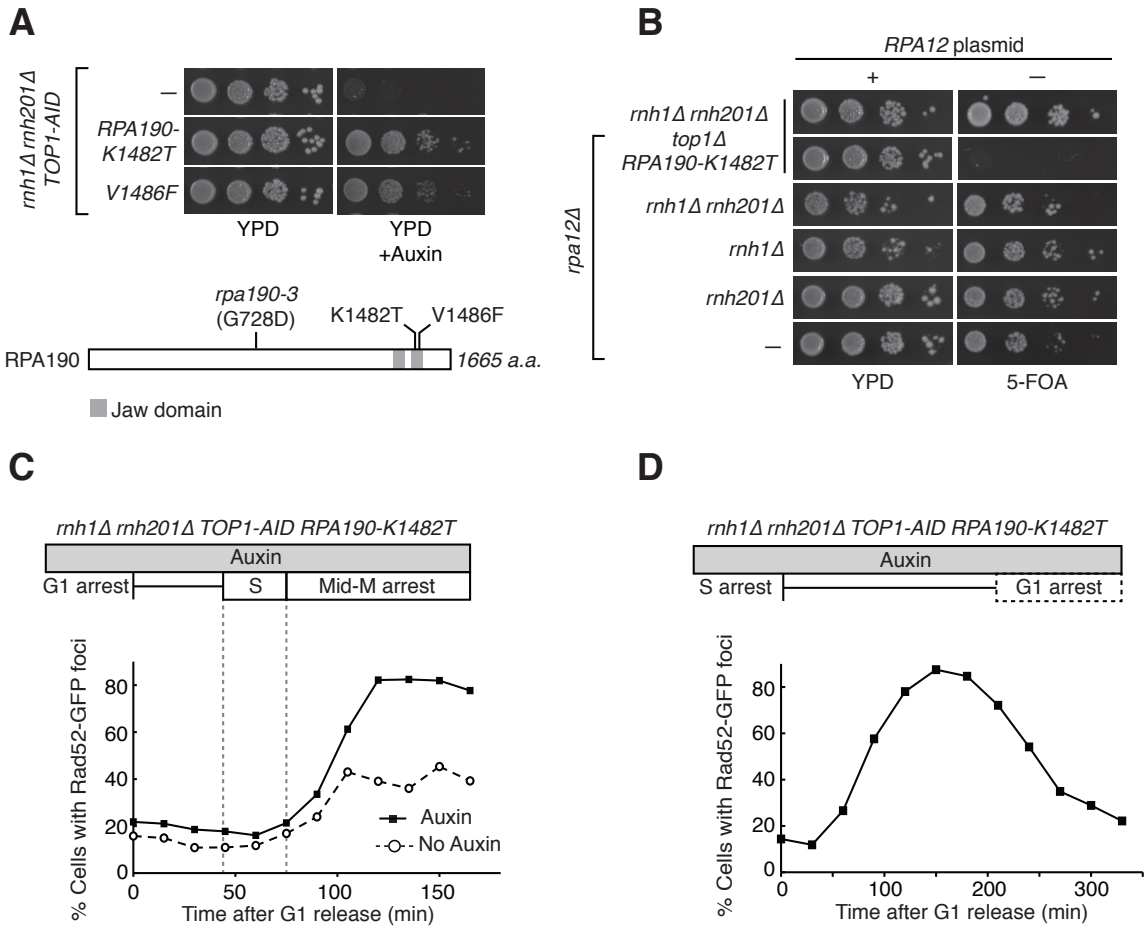

Figure 6 – *RPA190 mutants allow for repair of R-loop induced damage.* (A) *Top:* Rpa190-K1482T and -V1486F suppress auxin sensitivity of *rnh1*Δ *rnh201*Δ *TOP1-AID* cells. 10-fold serial dilutions of saturated cultures were plated onto YPD or YPD with auxin. *Bottom:* Schematic of Rpa190 showing the location of mutations and the jaw domain, as previously published [26,27]. (B) Rpa12 is required in *rnh1*Δ *rnh201*Δ *TOP1-AID RPA190-K1482T*. Cells carrying a plasmid expressing *RPA12* and *URA3* were plated onto media lacking uracil (-URA, selects for plasmid) or media containing 5-floroorotic acid (5-FOA, selects for plasmid loss). 10-fold serial dilutions are shown. (C) Rpa190-K1482T does not change accumulation of Rad52-GFP foci. Experiment in Figure 4A was repeated on *rnh1*Δ *rnh201*Δ *TOP1-AID RPA190-K1482T* cells. (D) Rpa190-K1482T allows for repair of Rad52-GFP foci. Experiment in Figure 2B was repeated on *rnh1*Δ *rnh201*Δ *TOP1-AID RPA190-K1482T* cells in the presence of auxin.

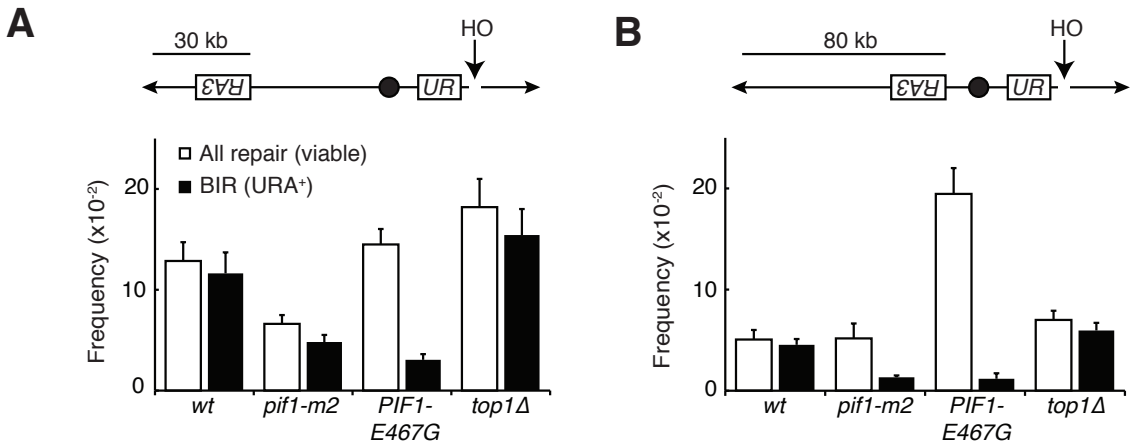

Figure 7 – *Pif1 mutants inhibit break-induced replication.* (A) *Top:* Schematic of 30kb repair template strain. The HO endonuclease is under control of a GAL promoter. In the presence of galactose, it is expressed, inducing a DSB on chromosome V. Sequences telomeric to the HO cut site are non-essential. Homology between the two incomplete *URA3* fragments allows for BIR and subsequent telomere addition. *Bottom:* Frequencies of repair. The percentage of cells that are viable on galactose (compared to total cells plated on non-DSB inducing YPD) indicates the frequency of all repair events. The subset of those cells that grow on media lacking uracil (URA^+) indicates the frequency of BIR events. (B) As in (A), but with a repair template 80kb from the telomere. Bars represent mean +/- standard deviation (*n=4*).

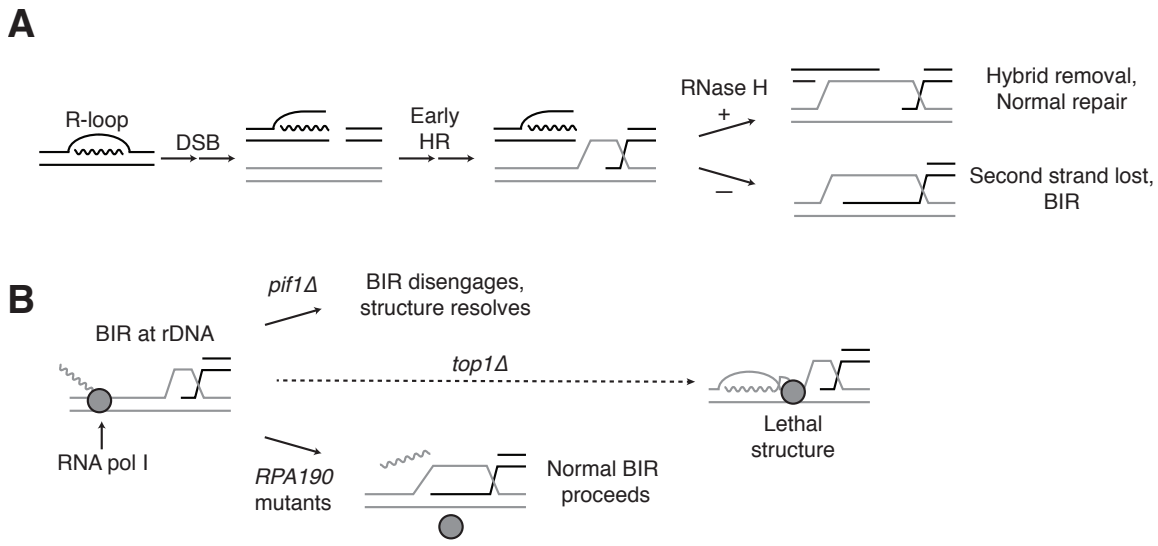

Figure 8 – *Proposed model for R-loop induced instability.* (A) R-loops that cause DSBs persist at the break site. Early HR events (resection, homology search, strand capture and invasion) proceed as normal for one side of the break, but are inhibited by the presence of an R-loop on the opposite side. If RNase H1 or H2 act to clear the hybrid, repair can proceed as normal. If the hybrid persists, the second strand cannot be captured and the cell engages BIR. (B) BIR at the rDNA encounters replication blocks and slows. These replication blocks (over/under-winding, transcribing or stalled RNA polI, R-loops) are exacerbated in the absence of Top1, creating unresolvable structures that lead to cell death. *PIF1* and *POL32* mutants make BIR less processive, allowing BIR machinery to disengage before lethality occurs. The repair mechanism used after BIR is disengaged is unknown. *RPA190* mutants allow for resolution of these structures, perhaps by disengaging RNA pol I through termination or backtracking activities.

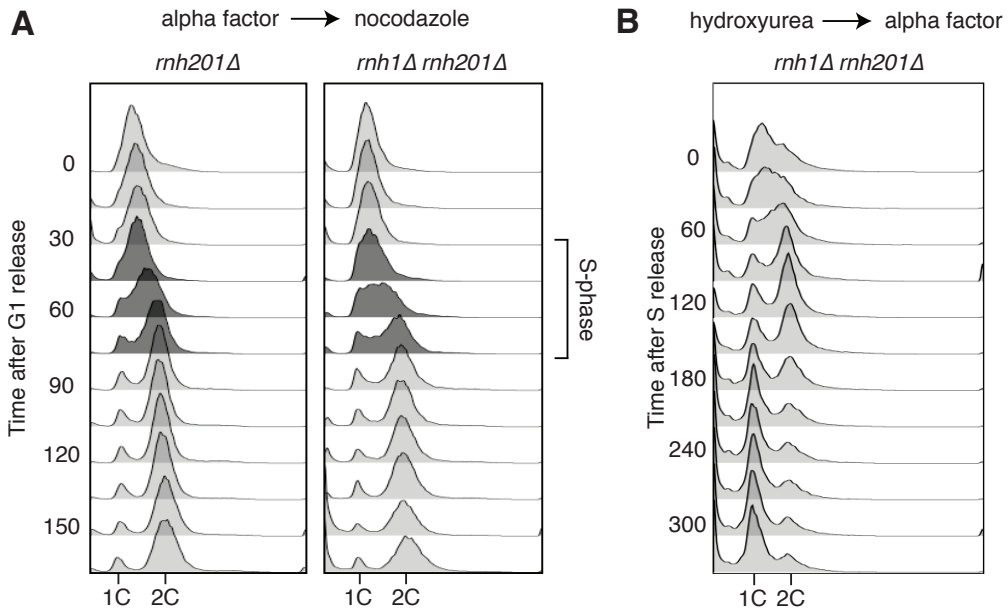

Supplemental Figure 1 – (A) Flow cytometry of *rnh201*Δ and *rnh1*Δ *rnh201*Δ cells released from alpha factor into nocodazole. Corresponds to figure 1C. (B) Flow cytometry of *rnh1*Δ *rnh201*Δ cells released from hydroxyurea into alpha factor. Corresponds to figure 2B.

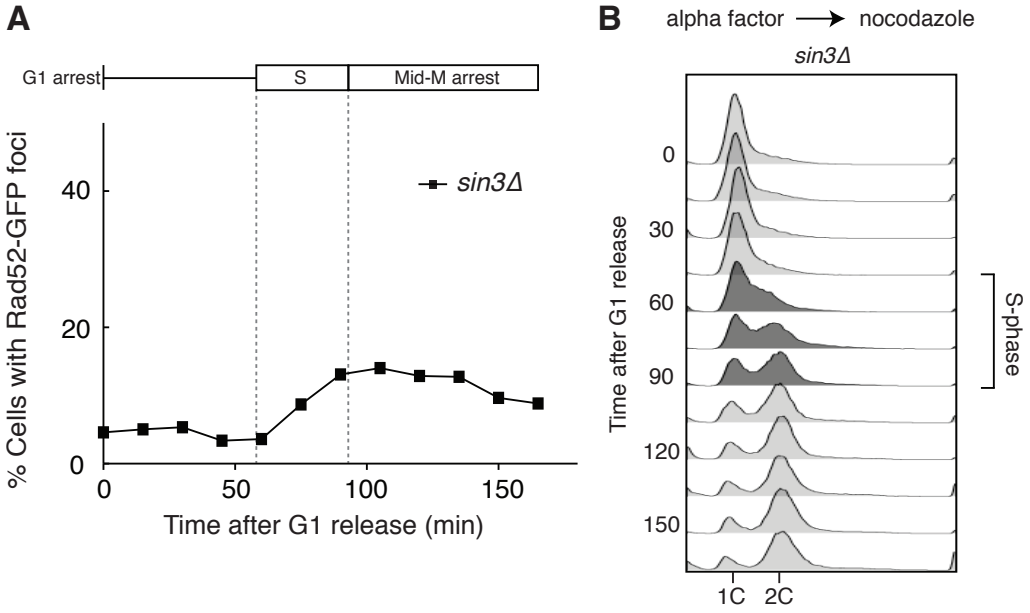

Supplemental Figure 2 – *Deleting SIN3 causes increased foci in S phase*. (A) Cultures of *sin3*Δ cells were arrested in alpha factor and released into nocodazole. Samples were taken at 15-minute intervals, and cells were scored for Rad52-GFP foci. (B) Flow cytometry of cells in (A).

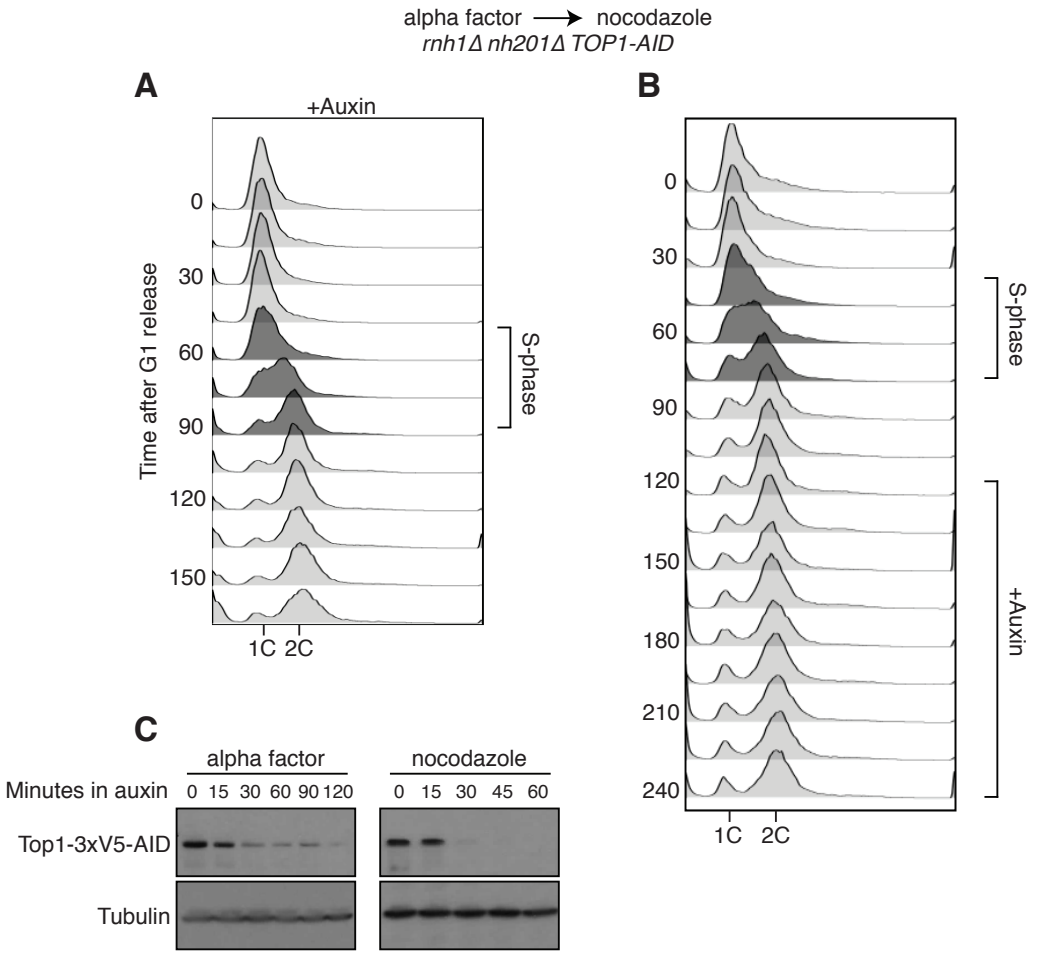

Supplemental Figure 3 – *Details on rnh1Δ rnh201Δ TOP1-AID cells released from alpha factor into nocodazole.* (A) Flow cytometry corresponds to figure 4A. Auxin is added to cells while they are arrested in alpha factor. Cells are then released into nocodazole and auxin, maintaining the state of Top1 depletion. (B) Flow cytometry corresponds to figure 4B. Auxin is added to cultures in nocodazole 120 minutes after release from alpha factor. (C) Cells arrested in alpha factor or nocodazole were treated with auxin. Samples were taken at the indicated time points and processed for western blotting. *Top:* Mouse anti-V5 antibody detects Top1-3xV5-AID. Addition of auxin depletes Top1 by two hours in alpha factor and 30 minutes in nocodazole. *Bottom:* Rabbit anti-tubulin antibody detects Tub1.

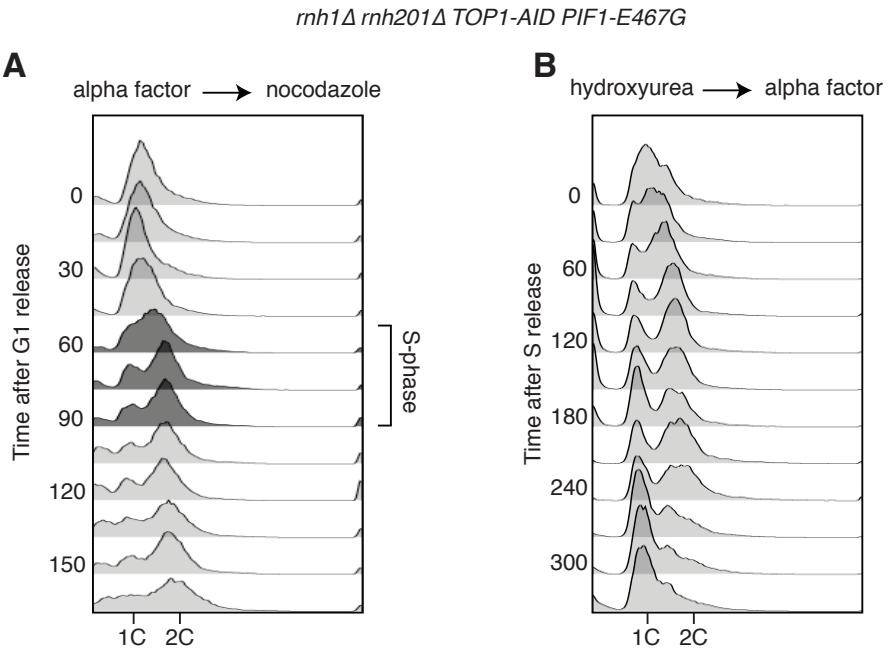

Supplemental Figure 4 – *Flow cytometry on rnh1Δ rnh201Δ TOP1-AID PIF1-E467G cells.* All cells have been treated with auxin for two hours before release and auxin is maintained in the culture after release. (A) Cells are released from alpha factor into nocodazole. Flow cytometry profiles correspond to figure 5C. (B) Cells are released from hydroxyurea into alpha factor. Corresponds to figure 5D.

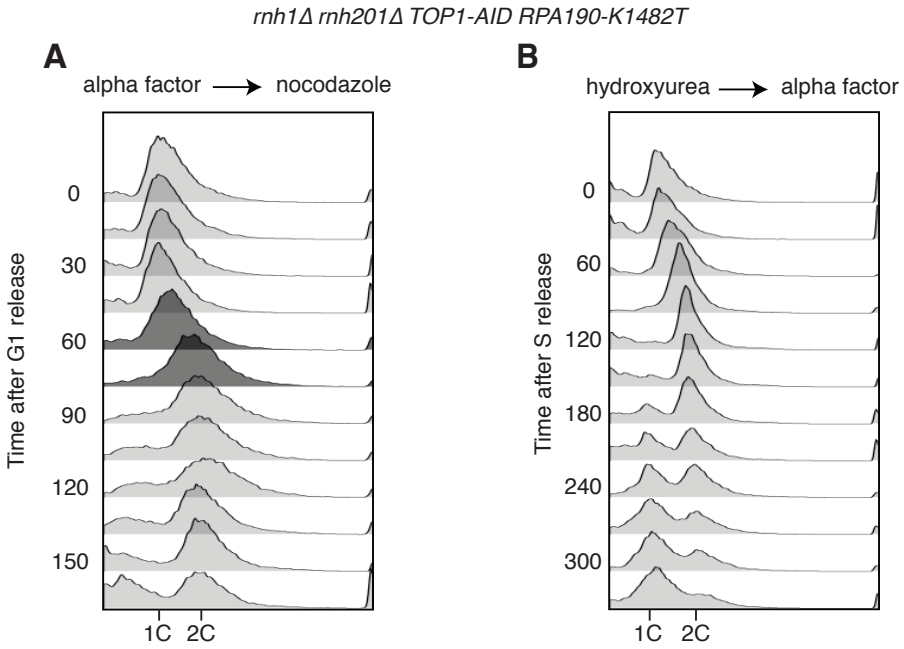

Supplemental Figure 5 – *Flow cytometry on rnh1Δ rnh201Δ TOP1-AID RPA190-K1482T cells.* All cells have been treated with auxin for two hours before release and auxin is maintained in the culture after release. (A) Cells are released from alpha factor into nocodazole. Flow cytometry profiles correspond to figure 6C. (B) Cells are released from hydroxyurea into alpha factor. Corresponds to figure 6D.

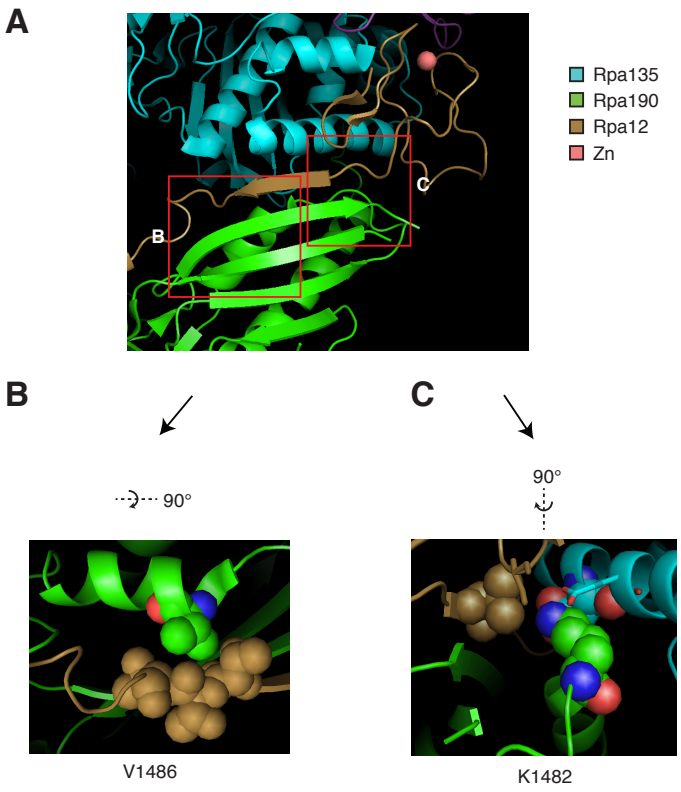

Supplemental Figure 6 – *Structural analysis of Rpa190 in the context of the RNA pol I complex*. Structure shown is from Protein Data Bank accession number 4C3I, as originally published in Fernández-Tornero, et al. (2013). (A) The "jaw" domain of Rpa190 (green) is shown with the N-terminal zinc-ribbon of Rpa12 (brown) and the "lobe" domain of Rpa135 (cyan). (B) The highlighted region rotated to see residue V1486 in its position on the alpha helix of RPA190 behind the beta sheet in the foreground of (A). Residue V1486 on Rpa190 is shown in spherical space along with residues T49, T50, and T51 of Rpa12. Steric clashes arise between these residues when Rpa190-V1486 is modified to phenylalanine. (C) The highlighted region rotated to see residue K1482 behind the beta sheet in the foreground of (A). Residue K1482 of Rpa190 is shown in spherical space along with Rpa135-D304 and Rpa12-V47 in the background. Also in close proximity are Rpa135-E307 and Rpa12-S6 shown as stick models in the foreground. Modifying Rpa190-K1482 to threonine increases the distance between these residues and possibly interrupts acid-base interactions anchored by the lysine residue.

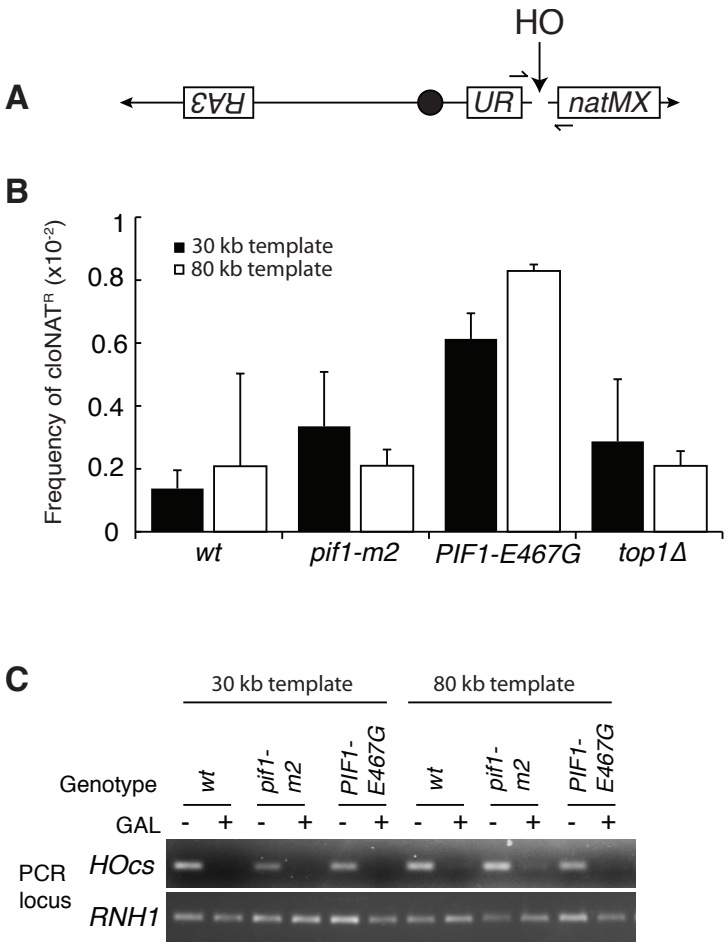

Supplemental Figure 7 – *Mutants don't affect non-homologous end joining or HO-induced DSBs* (A) More-detailed schematic of chromosome V constructs being used in Figure 7. A gene that confers resistance to the drug cloNAT (*natMX)* is placed telomeric to the HO cut site (HOcs). Primers designed to flank the HOcs are shown as well. (B) Frequencies of cloNAT resistance in various genotypes in both 30- and 80kb repair template strains. Viable colonies grown on galactose (Figure 7) were replica-plated to media containing cloNAT. Frequency is calculated by comparing cells that grew on cloNAT to total cells on YPD. Ability to grow on uracil and cloNAT resistance were mutually exclusive. Bars represent mean +/- standard deviation (*n=4*). (C) Saturated cultures of the indicated genotype were diluted into media containing dextrose or galactose and allowed to divide for six hours. Genomic DNA was extracted and PCR was performed at the HO cut site (HOcs) or the *RNH1* locus as a positive control. PCR products were loaded onto an agarose gel and stained with ethidium bromide.

Supplemental Table 1 - Strains used in this study

Strain	Genotype	Reference
JA30	*MAT**a** RAD52-GFP-HIS3*	
JA373a	*MAT**a** RAD52-GFP-HIS3 rnh1Δ::KAN*	
JA320a	*MAT**a** RAD52-GFP-HIS3 rnh201Δ::NAT*	
JA338a	*MAT**a** RAD52-GFP-HIS3 rnh1Δ::KAN rnh201Δ::NAT*	
JA426b	*MAT**a** RAD52-GFP-HIS3 rnh1Δ::KAN rnh201Δ::NAT rad9Δ::URA3*	
JA382	*MAT**a** rad52Δ::LEU2 pRS316-RAD52*	
JA378	*MAT**a** rad52Δ::LEU2 pRS316-RAD52 rnh1Δ::KAN*	
JA380	*MAT**a** rad52Δ::LEU2 pRS316-RAD52 rnh201Δ::NAT*	
JA376	*MAT**a** rad52Δ::LEU2 pRS316-RAD52 rnh1Δ::KAN rnh201Δ::NAT*	
JA249a	*MAT**alpha** rad9Δ::URA3*	
JA255a	*MAT**a** RAD52-GFP-LEU2 his3-Δ1::TIR1-HIS3 bar1Δ::hisG*	
JA268b	*MAT**a** RAD52-GFP-LEU2 his3-Δ1::TIR1-HIS3 bar1Δ::hisG sin3Δ::KAN*	
JA238	*MAT**a** RAD52-GFP-LEU2 his3-Δ1::TIR1-HIS3 bar1Δ::hisG-URA3-hisG*	
JA210	*MAT**alpha** RAD52-GFP-LEU2 his3-Δ1::TIR1-HIS3 bar1Δ::hisG-URA3-hisG TOP1-3xV5-AID-KAN*	
JA208	*MAT**a** RAD52-GFP-LEU2 his3-Δ1::TIR1-HIS3 bar1Δ::hisG-URA3-hisG TOP1-3xV5-AID-KAN rnh1Δ::HYG*	
JA209	*MAT**a** RAD52-GFP-LEU2 his3-Δ1::TIR1-HIS3 bar1Δ::hisG-URA3-hisG TOP1-3xV5-AID-KAN rnh201Δ::NAT*	
JA204a	*MAT**a** RAD52-GFP-LEU2 his3-Δ1::TIR1-HIS3 bar1Δ::hisG-URA3-hisG TOP1-3xV5-AID-KAN rnh1Δ::HYG rnh201Δ::NAT*	
JA214	*MAT**a** RAD52-GFP-LEU2 his3-Δ1::TIR1-HIS3 bar1Δ::hisG-URA3-hisG rnh201Δ::NAT*	
JA207	*MAT**a** RAD52-GFP-LEU2 his3-Δ1::TIR1-HIS3 bar1Δ::hisG-URA3-hisG rnh201Δ::NAT rnh1Δ::HYG*	
JA205	*MAT**a** RAD52-GFP-LEU2 bar1Δ::hisG-URA3-hisG rnh1Δ::HYG rnh201Δ::NAT*	
JA240	*MAT**a** RAD52-GFP-LEU2 his3-Δ1::TIR1-HIS3 bar1Δ::hisG TOP1-3xV5-AID-KAN rnh1Δ::HYG rnh201Δ::NAT*	
JA250a	same as JA240 except *rad9Δ::URA3*	
JA302a	same as JA240 except *RPA190-K1482T*	
JA303a	same as JA240 except *RPA190-V1486F*	
JA304a	same as JA240 except *PIF1-E467G*	
JA413a	same as JA240 except *pif1-m2*	
JA421a	same as JA240 except *pif1Δ::URA3*	
JA423a	same as JA240 except *pol32Δ::URA3*	
JA271a	*MAT**a** rnh1Δ::KAN rnh201Δ::NAT top1Δ::HYG RAD52-GFP-HIS3 pRS316-RNH1*	
JA308a	*MAT**a** rnh1Δ::HYG rnh201Δ::NAT top1Δ::HYG RAD52-GFP-HIS3 RPA190-K1482T*	
JA309b	*MAT**a** rnh1Δ::HYG rnh201Δ::NAT top1Δ::HYG RAD52-GFP-HIS3 RPA190-V1486F*	
JA310	*MAT**a** rnh1Δ::HYG rnh201Δ::NAT top1Δ::HYG RAD52-GFP-HIS3 RPA190-K1482T*	
JA394	*MAT**a** pRS316-RPA12 RAD52-GFP-HIS3 rpa12Δ::LEU2*	
JA392a	*MAT**a** pRS316-RPA12 RAD52-GFP-HIS3 rpa12Δ::LEU2 rnh1Δ::KAN*	

JA393a	*MAT**a** pRS316-RPA12 RAD52-GFP-HIS3 rpa12Δ::LEU2 rnh201Δ::NAT*	
JA390	*MAT**a** pRS316-RPA12 RAD52-GFP-HIS3 rpa12Δ::LEU2 rnh1Δ::KAN rnh201Δ::NAT*	
JA344a	*MAT**a** pRS316-RPA12 RAD52-GFP-HIS3 rpa12Δ::LEU2 rnh1Δ::KAN rnh201Δ::NAT top1Δ::HYG RPA190-K1482T*	
JA325a	*MAT**a** pRS316-RPA12 RAD52-GFP-HIS3 rnh1Δ::KAN rnh201Δ::NAT top1Δ::HYG RPA190-K1482T*	
yRA52	*MAT**a**::ΔHOcs::hisG ura3Δ851 trp1Δ63 leu2Δ::KAN hmlΔ::hisG HMR::ADE3 ade3::GAL::HO can1Δ::UR::HOcs::NAT, RA3::TRP1 (30kb)*	Anand, et al. 2014
JA415a	same as yRA52 except *pif1-m2*	
JA416a	same as yRA52 except *PIF1-E467G*	
JA447a	same as yRA52 except *top1Δ::HYG*	
yRA107	*MAT**a**::ΔHOcs::hisG ura3Δ851 trp1Δ63 leu2Δ::KAN hmlΔ::hisG HMR::ADE3 ade3::GAL::HO can1Δ::UR::HOcs::NAT, RA3::TRP1 (80kb)*	Anand, et al. 2014
JA417a	same as yRA107 except *pif1-m2*	
JA418a	same as yRA107 except *PIF1-E467G*	
JA448a	same as yRA107 except *top1Δ::HYG*	

Supplemental Table 2 - plasmids used in this study

Plasmid	Description	Reference
pRS316	*CEN ARS URA3* low copy plasmid	Lab stock
pRS306	*URA3* integrating plasmid	Lab stock
pRS316-*RAD52*	Rad52 complementation plasmid.	This study
pRS316-*RPA12*	Rpa12 complementation plasmid.	This study
pRS306-*RPA190-V1486F*	Integrating plasmid for creating *RPA190-K1482T*.	This study
pRS306-*RPA190-V1486F*	Integrating plasmid for creating *RPA190-V1486F*.	This study
pRS306-*PIF1-E467G*	Integrating plasmid for creating *PIF1-E467G*.	This study
pVS31	Integrating plasmid for creating *pif1-m2*	Schulz and Zakian, 1994

Materials and Methods

Yeast strains, media, and reagents
Details on strain genotypes can be found in Supplemental Table 1. Plasmids used in this study can be found in Supplemental Table 2. YPD and synthetic complete minimal media were prepared as previously described [38]. For all cultures and plates using auxin, a one molar stock of 3-indoleacetic acid (Sigma-Aldrich) in DMSO was made and added to a final concentration of 500 μM. All auxin-treated experiments were compared to experiments that were mock-treated with equivalent volumes of DMSO. 5-fluorooritc acid (US Biological) was used at a final concentration of 1 mg/ml (w/v).

Dilution plating assays
Cells were grown to saturation at 30°C in YPD. Cultures were then plated in 10-fold serial dilutions. Plates were incubated at 23°C. Representative images of experiments performed in duplicate or triplicate are shown.

Chromosome spreads
Cells were collected and spheroplasted (0.1 M potassium phosphate [pH 7.4], 1.2 M sorbitol, 0.5 mM $MgCl_2$, 20 mM DTT, 1.3 mg/ml zymolyase) at 37°C for 10 minutes or until >95% of cells lysed upon contact with 1% SDS. Spheroplasting reaction was stopped by washing and resuspension in a solution containing 0.1 M MES, 1 mM EDTA, 0.5 mM $MgCl_2$, and 1M sorbitol (pH 6.4). Spheroplasts were placed onto slides and simultaneously lysed (1% Lipsol [v/v]) and fixed (4% paraformaldehyde [w/v], 3.4% sucrose [w/v]) by spreading solutions together across the slides using a glass pipette. Slides were left to dry at room temperature overnight. Indirect immunofluorescence was then performed as previously described [7].

Synchronous releases
Cells were grown to mid-log phase at 23°C in YPD. For G1 releases, alpha factor (Sigma-Aldrich) was added to 10^{-8} M and cultures were incubated for approximately 3.5 hours, until >95% of cells were visually confirmed to be arrested in G1. Cultures were split and treated with auxin or mock treated for two hours. Cells were then collected and washed six times in 1mL of YPD containing 0.1 mg/ml Pronase E (Sigma-Aldrich), with or without auxin depending on treatment. Cells were then resuspended in YPD containing nocodazole (Sigma-Aldrich) at a concentration of 15 μg/ml, with or without auxin, depending on treatment. Cultures were then grown at 23°C.

For S-phase releases, cells were arrested in hydroxyurea (Sigma-Aldrich) at a final concentration of 200 mM for 3 hours at 23°C. Cultures were split and treated with auxin or mock treated for 1.5 hours. Cells were washed 6x 1mL with YPD and released into YPD containing 10^{-8} M alpha factor (with or without auxin, depending on treatment). Cultures were then grown at 23°C. Note that all strains used in time-courses were *bar1*Δ to allow for greater sensitivity to alpha factor.

Flow cytometry

Fixed cells were washed twice in 50 mM sodium citrate (pH 7.2), then treated with RNase A (50 mM sodium citrate [pH 7.2]; 0.25 mg/ml RNase A; 1% Tween-20 [v/v]) overnight at 37°C. Proteinase K was then added to a final concentration of 0.2 mg/ml and samples were incubated at 50°C for 2 hours. Samples were sonicated for 30s or until cells were adequately disaggregated. SYBR Green DNA I dye (Life Technologies) was then added at 1:20,000 dilution and samples were run on a Guava easyCyte flow cytometer (Millipore). 20,000 events were captured for each time point. Quantification was performed using FlowJo analysis software.

Microscopy

Asynchronously and synchronously dividing cells were collected and resuspended in fixative (paraformaldehyde 4% [w/v] and sucrose 3.4% [w/v]) for 15 minutes at room temperature followed by washing and storage in 0.1 M potassium phosphate (pH 7.4), 1.2 M sorbitol. When indicated, nuclei were visualized by brief permiabilization of fixed cells with 1% Triton X 100 (v/v) followed by staining with DAPI at final concentration of 1 μg/ml. Scoring and image acquisition was with an Axioplan2 microscope (100x objective, numerical aperture [NA] 1.40; Zeiss, Thornwood, NY) equipped with a Quantix CCD camera (Photometrics, Tucson, AZ).

Western blotting

Western blots were performed as previously described [39]. Primary antibodies used were a mouse monoclonal anti-V5 used at a 1:5000 dilution (Invitrogen) and a mouse monoclonal anti-Tub1 used at 1:20,000 dilution. Secondary antibody used was an HRP-conjugated goat anti-mouse at 1:20,000 (BioRad).

Genetic Screen

Multiple independent cultures of strain JA271a were grown to saturation in YPD to allow for loss of plasmid pRS316-RNH1 (*RNH1 CEN URA3*). Cultures were diluted and plated so that dozens of colonies formed on each plate. Frequency of 5-FOA resistance was approximately 10^{-7}. Colonies were then confirmed to be *rnh1*Δ *rnh201*Δ *top1*Δ, URA^-, *grande* (able to grow on glycerol as the sole carbon source, indicating functional mitochondria), and not carry any temperature sensitivities. Genomic DNA was extracted and libraries were prepared using an Illumina TruSeq kit. Libraries were multiplexed and sequenced with 14-fold minimal coverage. Sequences were mapped to an S288c reference genome and SNPs were called relative to the parental JA271a strain. All three suppressors discussed here were built into *rnh1*Δ *rnh201*Δ *top1*Δ strains to confirm genetic linkage before being built into *TOP1-AID* strains.

BIR assay

Experiments were performed as previously described [36]. Strains were grown on YPD +cloNAT plates. Individual colonies were picked and serially diluted in water so that ~200 cells were plated onto YPD and ~2000 cells were plated on YP-GAL. Cells that grew on YP-GAL were counted then replica-plated onto SC –URA and YPD +cloNAT plates. Total survivors were calculated by dividing the number of colonies that grew on

YP-GAL by the number that grew on YPD, adjusting for 10-fold dilution. Similar calculations were performed on SC –URA and YPD +cloNAT plates to determine rates of BIR and NHEJ, respectively.

References

1. Gaillard H, Aguilera A. Transcription as a Threat to Genome Integrity. Annu Rev Biochem. 2016;85: 291–317. doi:10.1146/annurev-biochem-060815-014908

2. Cerritelli SM, Crouch RJ. Ribonuclease H: the enzymes in eukaryotes. FEBS J. 2009;276: 1494–1505. doi:10.1111/j.1742-4658.2009.06908.x

3. Wahba L, Costantino L, Tan FJ, Zimmer A, Koshland D. S1-DRIP-seq identifies high expression and polyA tracts as major contributors to R-loop formation. Genes & Development. Cold Spring Harbor Lab; 2016;30: 1327–1338. doi:10.1101/gad.280834.116

4. Wahba L, Amon JD, Koshland D, Vuica-Ross M. RNase H and multiple RNA biogenesis factors cooperate to prevent RNA:DNA hybrids from generating genome instability. Mol Cell. 2011;44: 978–988. doi:10.1016/j.molcel.2011.10.017

5. O'Connell K, Jinks-Robertson S, Petes TD. Elevated Genome-Wide Instability in Yeast Mutants Lacking RNase H Activity. Genetics. Genetics; 2015;201: 963–975. doi:10.1534/genetics.115.182725

6. Warner JR. The economics of ribosome biosynthesis in yeast. Trends Biochem Sci. 1999;24: 437–440.

7. Wahba L, Gore SK, Koshland D. The homologous recombination machinery modulates the formation of RNA-DNA hybrids and associated chromosome instability. Elife. 2013;2: e00505. doi:10.7554/eLife.00505

8. Hage El A, French SL, Beyer AL, Tollervey D. Loss of Topoisomerase I leads to R-loop-mediated transcriptional blocks during ribosomal RNA synthesis. Genes & Development. 2010;24: 1546–1558. doi:10.1101/gad.573310

9. Stuckey R, García-Rodríguez N, Aguilera A, Wellinger RE. Role for RNA:DNA hybrids in origin-independent replication priming in a eukaryotic system. Proceedings of the National Academy of Sciences. National Acad Sciences; 2015;112: 5779–5784. doi:10.1073/pnas.1501769112

10. Ginno PA, Lott PL, Christensen HC, Korf I, Chédin F. R-loop formation is a distinctive characteristic of unmethylated human CpG island promoters. Mol Cell. 2012;45: 814–825. doi:10.1016/j.molcel.2012.01.017

11. Sun Q, Csorba T, Skourti-Stathaki K, Proudfoot NJ, Dean C. R-loop stabilization

represses antisense transcription at the Arabidopsis FLC locus. Science. American Association for the Advancement of Science; 2013;340: 619–621. doi:10.1126/science.1234848

12. Skourti-Stathaki K, Proudfoot NJ, Gromak N. Human Senataxin Resolves RNA/DNA Hybrids Formed at Transcriptional Pause Sites to Promote Xrn2-Dependent Termination. Mol Cell. 2011;42: 794–805. doi:10.1016/j.molcel.2011.04.026

13. Skourti-Stathaki K, Kamieniarz-Gdula K, Proudfoot NJ. R-loops induce repressive chromatin marks over mammalian gene terminators. Nature. 2014;516: 436–439. doi:10.1038/nature13787

14. Gómez-González B, Aguilera A. Activation-induced cytidine deaminase action is strongly stimulated by mutations of the THO complex. Proceedings of the National Academy of Sciences of the United States of America. 2007;104: 8409–8414. doi:10.1073/pnas.0702836104

15. Li X, Manley JL. Inactivation of the SR protein splicing factor ASF/SF2 results in genomic instability. Cell. 2005;122: 365–378. doi:10.1016/j.cell.2005.06.008

16. Ruiz JF, Gómez-González B, Aguilera A. AID Induces Double-Strand Breaks at Immunoglobulin Switch Regions and c-MYC Causing Chromosomal Translocations in Yeast THO Mutants. PLoS Genet. 2011;7: e1002009. doi:10.1371/journal.pgen.1002009.g005

17. Aguilera A, García-Muse T. R loops: from transcription byproducts to threats to genome stability. Mol Cell. 2012;46: 115–124. doi:10.1016/j.molcel.2012.04.009

18. Lisby M, Rothstein R, Mortensen UH. Rad52 forms DNA repair and recombination centers during S phase. Proceedings of the National Academy of Sciences of the United States of America. 2001;98: 8276–8282. doi:10.1073/pnas.121006298

19. Lisby M, Mortensen UH, Rothstein R. Colocalization of Multiple DNA double-strand breaks at a single Rad52 repair centre. Nature Cell Biology. 2003;5: 572–577.

20. Lazzaro F, Novarina D, Amara F, Watt DL, Stone JE, Costanzo V, et al. RNase H and Postreplication Repair Protect Cells from Ribonucleotides Incorporated in DNA. Mol Cell. 2012;45: 99–110. doi:10.1016/j.molcel.2011.12.019

21. Weinert TA, Hartwell LH. The RAD9 gene controls the cell cycle response to DNA damage in Saccharomyces cerevisiae. Science. 1988;241: 317–322.

22. Drolet M, Phoenix P, Menzel R, Massé E, Liu LF, Crouch RJ. Overexpression of RNase H partially complements the growth defect of an Escherichia coli delta

topA mutant: R-loop formation is a major problem in the absence of DNA topoisomerase I. Proceedings of the National Academy of Sciences of the United States of America. 1995;92: 3526–3530.

23. Massé E, Drolet M. Escherichia coli DNA topoisomerase I inhibits R-loop formation by relaxing transcription-induced negative supercoiling. J Biol Chem. 1999;274: 16659–16664.

24. Boulé J-B, Zakian VA. Roles of Pif1-like helicases in the maintenance of genomic stability. Nucleic Acids Research. Oxford University Press; 2006;34: 4147–4153. doi:10.1093/nar/gkl561

25. Schulz VP, Zakian VA. The saccharomyces PIF1 DNA helicase inhibits telomere elongation and de novo telomere formation. Cell. 1994;76: 145–155.

26. Engel C, Sainsbury S, Cheung AC, Kostrewa D, Cramer P. RNA polymerase I structure and transcription regulation. Nature. 2013;502: 650–655. doi:10.1038/nature12712

27. Fernández-Tornero C, Moreno-Morcillo M, Rashid UJ, Taylor NMI, Ruiz FM, Gruene T, et al. Crystal structure of the 14-subunit RNA polymerase I. Nature. 2013;502: 644–649. doi:10.1038/nature12636

28. Wittekind M, Dodd J, Vu L, Kolb JM, Buhler JM, Sentenac A, et al. Isolation and characterization of temperature-sensitive mutations in RPA190, the gene encoding the largest subunit of RNA polymerase I from Saccharomyces cerevisiae. Molecular and Cellular Biology. 1988;8: 3997–4008.

29. Kuhn C-D, Geiger SR, Baumli S, Gartmann M, Gerber J, Jennebach S, et al. Functional architecture of RNA polymerase I. Cell. 2007;131: 1260–1272. doi:10.1016/j.cell.2007.10.051

30. Martinez-Rucobo FW, Cramer P. Structural basis of transcription elongation. Biochim Biophys Acta. 2013;1829: 9–19. doi:10.1016/j.bbagrm.2012.09.002

31. Dutta D, Shatalin K, Epshtein V, Gottesman ME, Nudler E. Linking RNA Polymerase Backtracking to Genome Instability in E. coli. Cell. 2011;146: 533–543. doi:10.1016/j.cell.2011.07.034

32. Malkova A, Naylor ML, Yamaguchi M, Ira G, Haber JE. RAD51-dependent break-induced replication differs in kinetics and checkpoint responses from RAD51-mediated gene conversion. Molecular and Cellular Biology. American Society for Microbiology; 2005;25: 933–944. doi:10.1128/MCB.25.3.933-944.2005

33. Saini N, Ramakrishnan S, Elango R, Ayyar S, Zhang Y, Deem A, et al. Migrating bubble during break-induced replication drives conservative DNA synthesis.

Nature. 2013;502: 389–392. doi:10.1038/nature12584

34. Davis AP, Symington LS. RAD51-dependent break-induced replication in yeast. Molecular and Cellular Biology. 2004;24: 2344–2351. doi:10.1128/MCB.24.6.2344-2351.2004

35. Wilson MA, Kwon Y, Xu Y, Chung W-H, Chi P, Niu H, et al. Pif1 helicase and Polδ promote recombination-coupled DNA synthesis via bubble migration. Nature. 2013;502: 393–396. doi:10.1038/nature12585

36. Anand RP, Tsaponina O, Greenwell PW, Lee C-S, Du W, Petes TD, et al. Chromosome rearrangements via template switching between diverged repeated sequences. Genes & Development. Cold Spring Harbor Lab; 2014;28: 2394–2406. doi:10.1101/gad.250258.114

37. Jain S, Sugawara N, Lydeard J, Vaze M, Tanguy Le Gac N, Haber JE. A recombination execution checkpoint regulates the choice of homologous recombination pathway during DNA double-strand break repair. Genes & Development. Cold Spring Harbor Lab; 2009;23: 291–303. doi:10.1101/gad.1751209

38. Guacci V, Koshland D, Strunnikov A. A direct link between sister chromatid cohesion and chromosome condensation revealed through the analysis of MCD1 in S. cerevisiae. Cell. 1997;91: 47–57.

39. Eng T, Guacci V, Koshland D. Interallelic complementation provides functional evidence for cohesin-cohesin interactions on DNA. Molecular Biology of the Cell. American Society for Cell Biology; 2015;26: 4224–4235. doi:10.1091/mbc.E15-06-0331

Chapter III. Depletion of RNases H1 and H2

Introduction

Figure 4C in chapter II of this dissertation shows that *rnh1*Δ *rnh201*Δ *TOP1-AID* cells do not recover from auxin treatment. It is important to note that this was a transient, four-hour Top1-AID depletion – cells were treated with auxin, washed, and then plated on YPD, thereby allowing Top1-AID levels to return to normal. We concluded that a lethal event occurs when Top1 is depleted in *rnh1*Δ *rnh201*Δ cells that cannot be reversed by recovery of the Top1 protein. Together with our suppressor data, we reason that if Top1 is absent for long enough, BIR is fully engaged, collisions occur with RNA pol I, and cells pass a "point of no return."

We wished to ask whether this point of no return could be avoided by resolving R-loops. Adding topoisomerase I back into the cell after a certain point did not make repair possible, but could adding RNase H1 or H2 back rescue cells? Additionally, we wished to create a single-cell cycle system with conditional RNase H1 or H2, so we could ask more direct questions about R-loop formation and genome instability without having to worry about the potentially confounding effects of Top1 depletion. In this chapter, we briefly summarize a series of experiments performed in attempt to deplete RNases H1 and H2 with the auxin degron system. In short, these experiments failed in a way that was difficult to draw satisfying conclusions. However, there are several potential uses for conditional RNase H mutants, and they would be valuable reagents for the study of how R-loops affect DNA damage and repair. As such, in the hopes that future attempts at creating these reagents will be more successful, this is a record of what has been already tested.

Results

We began by creating auxin-tagged versions of Rnh1 and Rnh201 in *rnh201*Δ *top1*Δ and *rnh1*Δ *top1*Δ strains, respectively. Tagging Rnh1 at the C-terminus appeared to destabilize it, resulting in lower protein levels and high Rad52-GFP foci, even in the absence of auxin (Figure 1). We therefore used internally tagged versions of RNase H1, all of which were placed just after the proline at position 85. This position was chosen because it is found in the highly divergent linker region of RNase H1 and was therefore less likely to perturb functionally important structures. We have shown that tags at this region have no measurable effect on various phenotypes – Rad52-GFP foci in *rnh201*Δ cells, and viability in *rnh201*Δ *top1*Δ cells. Tagging Rnh201 at the C-terminus did not appear to cause any change in phenotypes (data not shown). For ease of notation, we will refer to internal tags with a semicolon (e.g. Rnh1;AID) as opposed to a hyphen, which here specifically indicates a C-terminal tag (e.g. Rnh201-AID).

As seen in Figure 2, depletion of Rnh1;AID in *rnh201*Δ *top1*Δ cells causes neither inviability nor an increase in Rad52-GFP foci, even after 12 hours of treatment with auxin. Depletion of Rnh201-AID in *rnh1*Δ *top1*Δ cells caused an extremely mild increase in inviability. Rad52-GFP foci in this strain increased slowly over the course of 12 hours to approximately 30%. This was a striking absence of phenotype when compared to Top1-AID in *rnh1*Δ *rnh201*Δ cells, which were inviable on auxin and had the expected increase in Rad52-GFP foci to around 80%. Both tagged proteins appeared to respond to auxin treatment and were depleted well below their normal levels. However, upon overexposure of these western blots, some protein remained.

We asked if this low level of remaining RNase H was responsible for preventing the phenotypes of lethality and ~80% Rad52-GFP foci. To further suppress the level of RNase H1 in the cell, we placed an inducible GAL promoter in front of the *RNH1;AID* locus. When cells were grown with galactose as a carbon source, Rnh1;AID would be overexpressed. When grown with dextrose, transcription at this locus would shut off. In addition, auxin could be added to the growth media to deplete any protein that happened to get translated. This method had two advantages. First, it acted as a "double knockdown" method. The use of both catabolite repression and auxin-inducible degradation together drops levels of Rnh1 protein below the level of either one of these methods used singly. Second, this method allows for relatively rapid control of both transcription and protein levels.

Surprisingly, even in the presence of both dextrose and auxin, *GAL:RNH1;AID rnh201*Δ *top1*Δ cells were still viable (Figure 3). This is despite the fact that growing cells in galactose overnight without auxin drops RNase H1 below detectable levels (Figure 3, bottom, lane 2). Switching cells from growth in galactose to dextrose and auxin effectively depleted RNase H1 levels, but perhaps not as rapidly as hoped. Overexposure of a western blot showed that some residual protein remained even after 8 hours in dextrose and auxin (Figure 3, bottom, lanes 3 and 4). Accumulation of Rad52-GFP in *rnh201*Δ cells depleted of RNase H1 was similar in both the presence and absence of topoisomerase I. Rad52-GFP foci from cells collected after a switch from galactose to dextrose and auxin slowly increased to approximately 30%, as seen before for depletion of RNase H2 (Figure 4). This relatively low level of Rad52-GFP foci was not a result of overnight growth in galactose, as endpoint analysis of cells grown overnight in dextrose had Rad52-GFP foci that accumulated to a similar level (data not shown). Taken together, this indicated that cells were responding neither as severely nor as rapidly to RNase H depletion as they were to topoisomerase I depletion in the previous chapter.

The slow accumulation of Rad52-GFP foci suggested that R-loops may be slow to accumulate as well. Furthermore, the absence of extreme phenotypes after depletion of RNase H1 in *rnh201*Δ *top1*Δ cells indicated that perhaps residual RNase H1 activity was preventing hybrids from accumulating. To determine the status of DNA:RNA hybrid accumulation, we grew *GAL:RNH1;AID rnh201*Δ cells in galactose then switched them to dextrose and auxin. Cells were collected every hour then processes for chromosome spreads and staining with the S9.6 antibody. Surprisingly, DNA:RNA hybrids appeared after two hours. Despite the presence of DNA:RNA hybrids, Rad52-GFP foci didn't begin to accumulate until four hours after switching media (Figure 4). Taken together,

depletion of RNase H1 in *rnh201*Δ cells allows for bulk R-loop accumulation, but there is a delay before Rad52-GFP foci accumulate.

Discussion

Here, we tested several AID-based systems for depleting the RNases H. Overall, no tagging or expression construct created robust, rapidly inducible phenotypes. Of the constructs tested, depletion of C-terminally tagged Rnh201 and internally tagged Rnh1 under control of a GAL promoter appeared to be somewhat effective, albeit slow. We did not attempt to put C-terminally tagged Rnh201 under control of a GAL promoter. Given the results from this section, we would not expect GAL shutoff of *RNH201* to further exacerbate any phenotypes, but this remains a potential route for future experimentation.

These particular auxin depletion constructs were ineffective for two reasons. First, phenotypes were marginal at best. The absence of topoisomerase I in an *rnh1*Δ *rnh201*Δ background has been thoroughly shown to be lethal in our lab and others. We have confirmed this lethality using three separate methods – by auxin depletion (see chapter II), shuffle plasmid (as in the genetic screen, see chapter II and appendix I), and breeding (data not shown). It is therefore surprising that depletion of RNase H1 and H2 doesn't induce lethality in the absence of Top1. This is despite low levels of residual protein – signals on western blots were either very low, as in the case of Rnh201-AID depletion, or undetectable, as in the case of Rnh1;AID depletion after GAL repression.

One interpretation of these results is that low and/or transient presence of RNase H activity is enough to prevent the lethal recombination structures proposed in chapter II. Figure 3 of the previous chapter shows that the presence of a single RNase H can completely suppress the extreme phenotypes (lethality, high Rad52-GFP foci, Rad9-dependent G2-M arrest) of the *rnh1*Δ *rnh201*Δ *top1*Δ mutant. Compare this to the presence of topoisomerase I, which can suppress lethality but only reduces Rad52-GFP foci by about 50%. Taken together, this suggests that the RNases H are far more effective at preventing R-loop induced damage that topoisomerase I.

Second, even when there was a mild phenotype – as in the 30% of cells with Rad52-GFP foci after RNase H1 depletion in *rnh201*Δ cells – this phenotype did not occur within one cell cycle. It is therefore difficult to conclude whether these foci had accumulated over one or several cell cycles. It would be interesting to perform cell cycle experiments on RNase H1 depleted *rnh201*Δ cells and see if the foci cycle as they do in *rnh1*Δ *rnh201*Δ cells. Regardless, the inability to control R-loop induced instability within one cell cycle greatly diminished the utility of these alleles.

Interestingly, there is an absence of a lethal phenotype despite the fact that R-loops accumulate. This could be an issue of resolution – while it appears that R-loops are accumulating, they are not doing so at a few specific loci. Higher resolution mapping techniques would need to be used to address this caveat. Alternatively, R-loops increase genome wide but are only converted to damage at a few loci. In either of these cases, if RNase H1 is easily recruited to specific loci, very little of the enzyme may be required to either prevent R-loop accumulation or their conversion to DNA damage. A third possibility is that R-loops are being turned over rapidly. In this case, low levels of RNase

H activity allow R-loops to accumulate but not persist, and only persistent R-loops lead to DNA damage.

Ultimately, despite its ineffectiveness in depleting RNase H1, the GAL/AID system used here could be a useful reagent for depletion of other proteins. Plasmid pL16-GAL-ScAID2 in *E. coli* strain JA1023 can be used for creating N-terminally AID tagged proteins under the control of a GAL promoter using simple PCR-based methods.

Figures

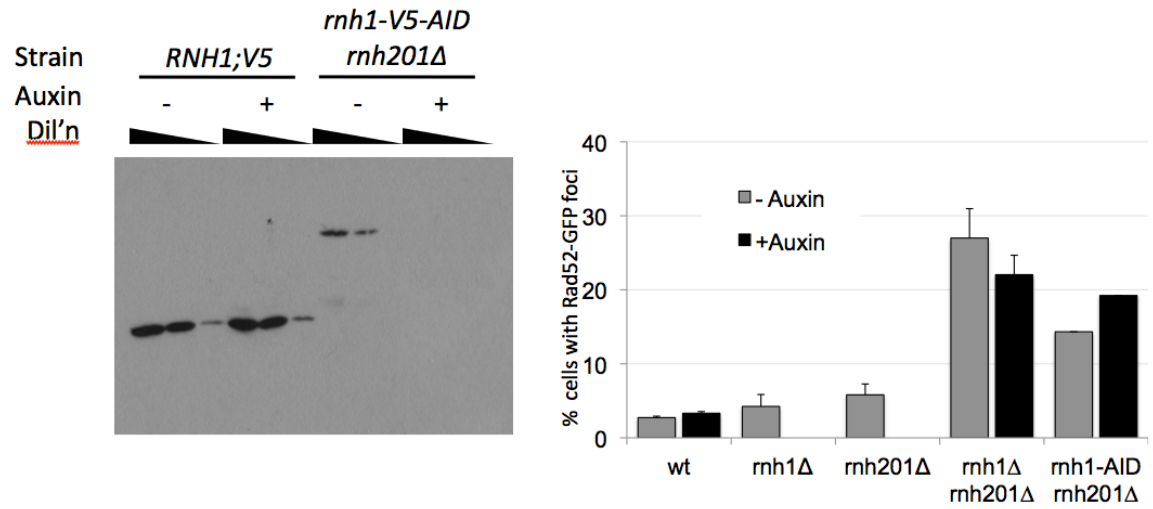

Figure 1 – *C-terminally tagged RNase H1 is hyopmorphic*. *Left* – Western blot showing internally-tagged RNase H1 (Rnh1*;*V5, left six lanes) compared to C-terminally auxin tagged RNase H1 (Rnh1-V5-AID, right six lanes) with and without auxin treatment. Dilutions are 2-fold and 10-fold, relative to the first lane in each group of three. The AID tag increases the size of the protein by approximately 25 kD. *Right* – Rad52-GFP foci were scored in cells of the indicated genotype, with and without auxin treatment.

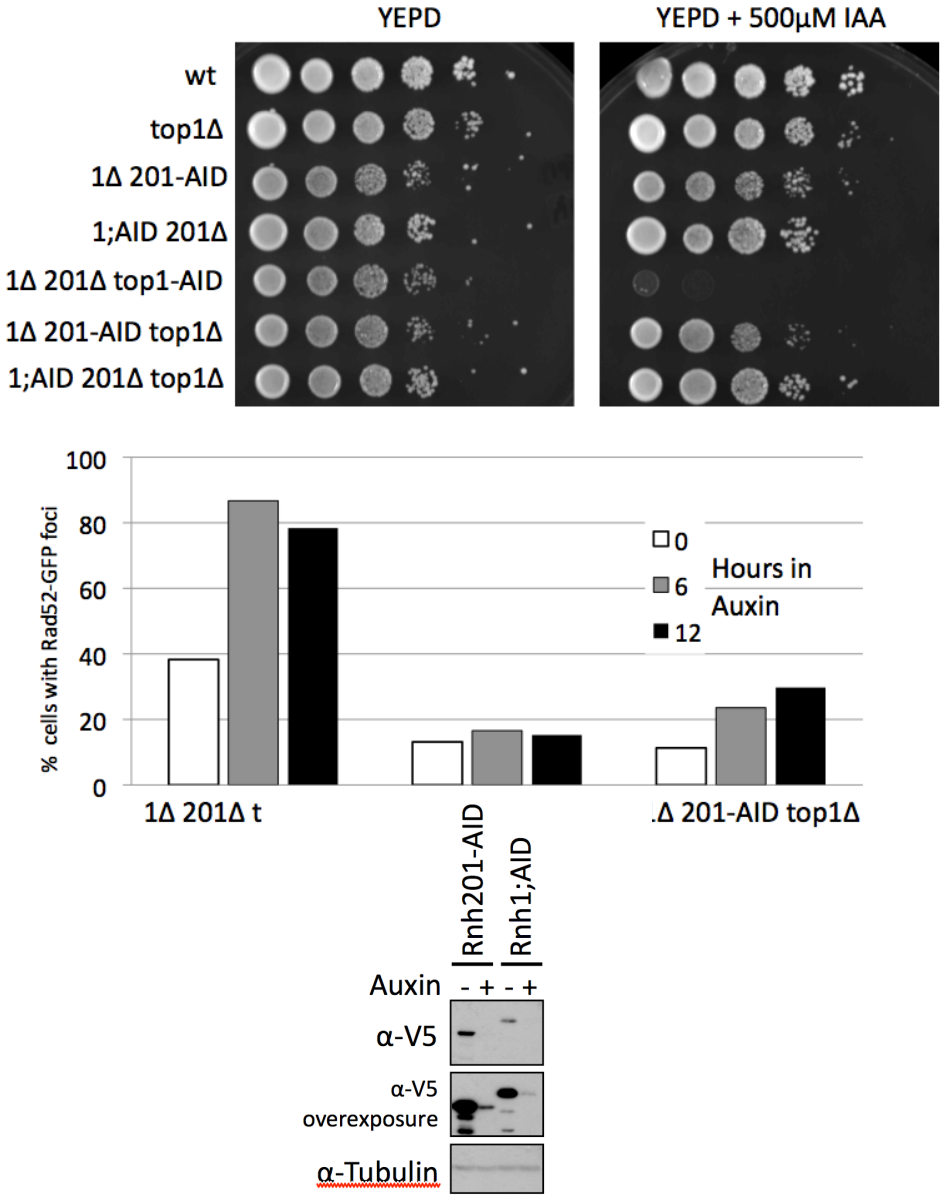

Figure 2 – *Depletion of RNases H in double mutants does not induce inviability or increase in Rad52-GFP foci. Top* – 10-fold serial dilutions of the three different AID constructs built into the relevant double and single mutants plated on YPD or YPD containing auxin. 1Δ – RNase H1 knockout; 201-AID – Rnh201 C-terminally tagged construct; 1;AID – Rnh1 internally tagged construct; 201Δ – RNase H2 knockout. *Middle* – Strains containing the three different AID constructs built into the relevant double mutant were treated with auxin for 0, 6, or 12 hours before collection and Rad52-GFP foci scoring. *Bottom* – Western blots showing depletion of Rnh201-3xV5-AID and Rnh1;3xV5-AID. Tubulin was blotted as a loading control.

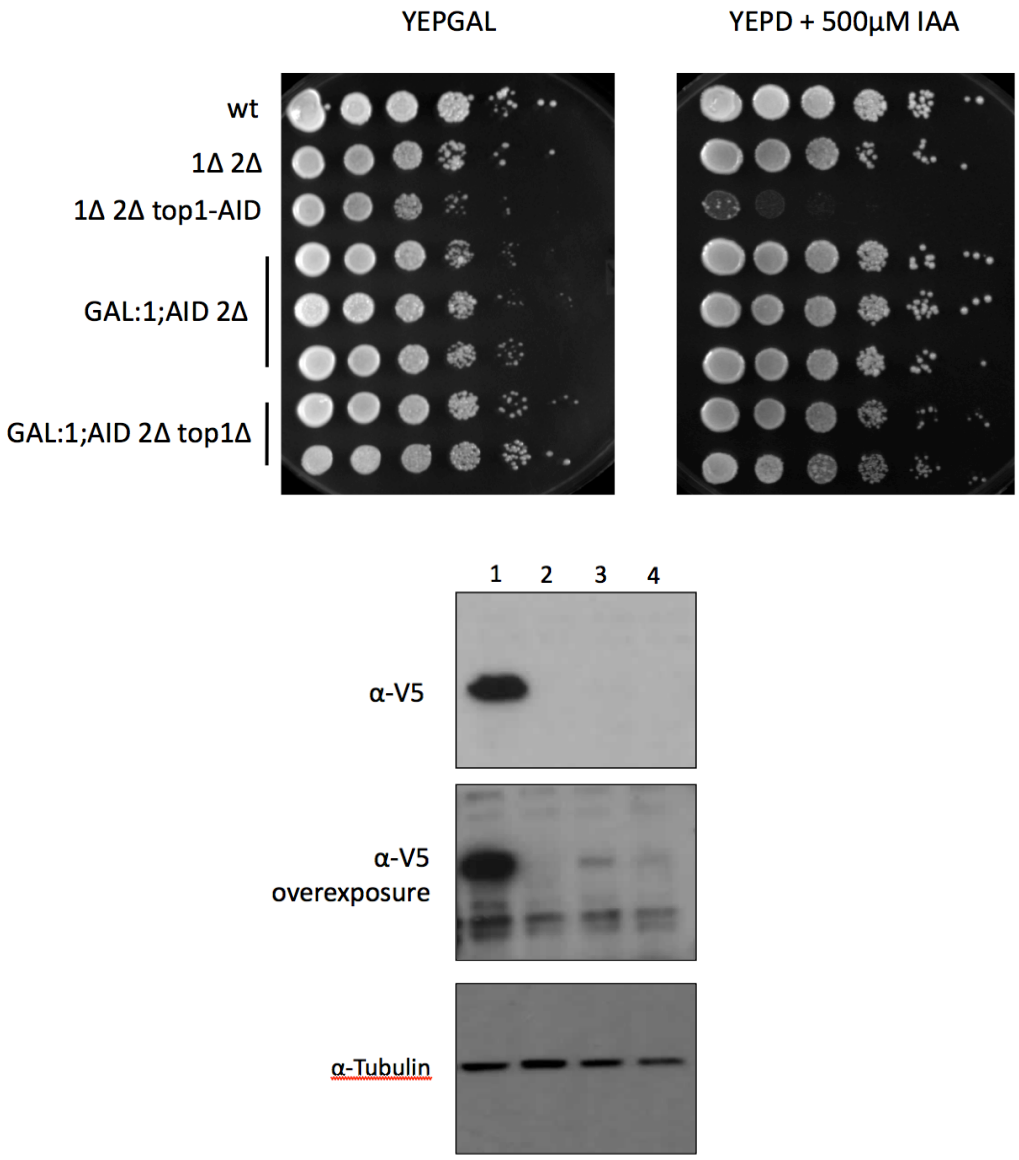

Figure 3 – *Depletion and catabolite repression of RNase H1 in rnh201Δ top1Δ cells does not cause inviability. Top* – Ten-fold serial dilutions of the indicated strain plated on media containing galactose or media containing dextrose and auxin. Abbreviations are the same as in Figure 2, except GAL:1;AID indicates RNaseH1 with an internal auxin tag under the control of a GAL promoter. *Bottom* – western blots showing depletion of RNase H1. Lane 1, Rnh1;V5-AID under control of a native promoter. Lane 2, Rnh1;V5-AID under control of a GAL promoter, grown overnight in dextrose. Lanes 3 and 4, Rnh1;V5-AID under control of a GAL promoter, grown overnight in galactose and switched to media containing dextrose and auxin. Lane 3, two hours after switch. Lane 4, eight hours after switch.

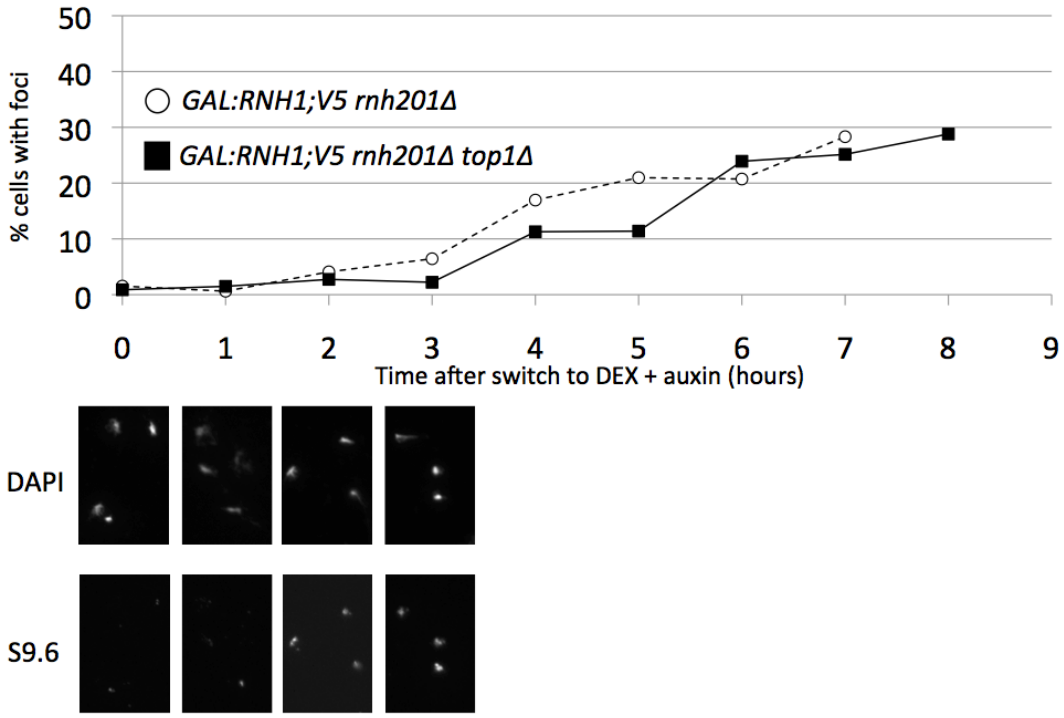

Figure 4 – *Depleting cells of RNase H1 causes DNA:RNA hybrids to appear before Rad52-GFP foci. Top* – Indicated strains were grown overnight in galactose then switched to media containing dextrose and auxin. Samples were taken every hour and scored for Rad52-GFP foci. *Bottom* – Cells from the *GAL:RNH1;V5 rnh201*Δ time course above were processed for chromosome spreads. DAPI shows nuclear staining and S9.6 shows the presence of DNA:RNA hybrids. Each image corresponds to the data point in the graph directly above it.

Supplemental Table 1 - Strains used in this study

Strain	Genotype	Note
JA239a	*MAT**a** rnh201Δ::NAT his3-Δ1::TIR1-HIS3 bar1Δ::hisG-URA3-hisG RAD52-GFP-LEU2 RNH1-3xV5-AID-KAN*	Rnh1 C-terminal tag
JA265a	same as JA239a but *top1Δ::HYG*	
JA248	*MAT**a** rnh201Δ::NAT his3-Δ1::TIR1-HIS3 bar1Δ::hisG RAD52-GFP-LEU2 RNH1;3xV5-AID*	Rnh1 internal AID tag
JA251a	same as JA248 but *top1Δ::HYG*	
JA298a	same as JA248 but *KAN-GAL1:RNH1;3xV5-AID*	
JA300a	same as JA298a but *top1Δ::HYG*	
JA243c	*MAT**a** rnh1Δ::HYG his3-Δ1::TIR1-HIS3 bar1Δ::hisG-URA3-hisG RAD52-GFP-LEU2 RNH201-3xV5-AID-KAN*	Rnh201 C-terminal tag
JA254a	same as JA243c but *top1Δ::HYG*	
JA270	*MAT**a** rnh1Δ::HYG his3-Δ1::TIR1-HIS3 bar1Δ::hisG-URA3-hisG RAD52-GFP-LEU2 RNH201-3xHA-AID2-KAN*	Rnh201 AID2 tag variant
JA287	same as JA270 but *top1Δ::NAT*	
JA150	*MAT**a** RNH1;3xV5*	

Supplemental Table 2 - plasmids used in this study

Plasmid	Description
pRS306-yRNH1;3xV5	Integrating plasmid to create Rnh1 internally tagged with 3xV5
pRS306-yRNH1;3xV5-AID1	Integrating plasmid to create Rnh1 internally tagged with 3xV5-AID
pL16-GAL-ScAID2	For creating N-terminal ScAID2 tagged proteins under the control of a GAL promoter (G418 marker)

Chapter IV. Conclusion

Several questions raised by this research could be exciting avenues for future studies. First and foremost, while we have shown that R-loops can affect DNA repair, the precise nature of the initial damage event remains a mystery. The timing of the accumulation and dissolution of Rad52-GFP foci in *rnh1*Δ *rnh201*Δ puts temporal constraints on when DNA damage and repair are occurring. Because the vast majority of Rad52-GFP foci accumulate after completion of S-phase, we conclude that challenges to repair are limited to G2/M. Moreover, the ability to induce new foci by depleting Top1 in *rnh1*Δ *rnh201*Δ cells suggests that damage can occur in G2/M as well, after bulk DNA replication has completed. This is in conflict with current models of R-loop mediated DNA damage, which propose that damage occurs in S-phase when an R-loop creates a barrier to an advancing replication fork.

What is the initial damage event if it is occurring after S-phase is complete? The most exotic explanation, consistent with the robust DNA damage response in G2/M, is that a double-stranded break is forming independently of DNA replication. It is currently not well understood how R-loops could form DSBs without replication fork collisions. Furthermore, if R-loop dependent DSBs can independently of S-phase, why don't they arise in G1 in addition to G2/M? Potential solutions involve cell-cycle dependent nucleases or other DNA metabolic factors. Perhaps further screening for suppressors of *rnh1*Δ *rnh201*Δ *top1*Δ lethality will uncover mutants that suppress the initial damage event, as opposed to enabling repair. These mutants could inform us about the *trans* factors that lead to DSBs.

It is important to note that we cannot entirely rule out a replication-dependent DSB. The rDNA is known to replicate late in S-phase, and late firing of ribosomal origins along with slow or stalling polymerases could translate to stretches of DNA that are still being replicated long after bulk S-phase has been completed. These late replication forks could collide with obstacles at the rDNA and cause DSBs. Alternatively, several studies have explored how Rad52-mediated HR, and specifically BIR, can help restart a stalled or fully collapsed replication fork. In this case, no proper DSB is formed, but the two new DNA strands of a stalled replication fork are treated similarly to a DSB.

A second potential area of future research involves the role of R-loops at the rDNA locus. Due to Top1's role in maintaining genome stability at the rDNA and the fact that spontaneous suppressors were found in RNA Pol I, it is likely that the repair centers seen here are largely occurring at the rDNA locus on chromosome XII. The rDNA poses specific challenges to DNA replication and repair due to its repetitive nature, tendency to form R-loops, and high transcriptional load. Which of these factors makes it so susceptible to R-loop induced instability? The Fob1/RFB system of rDNA repeat expansion and contraction is a prime suspect. Perhaps knocking out Fob1, thereby preventing rDNA recombination, would lower R-loop dependent DNA damage. Alternatively, adjusting the number of repeats in the rDNA cluster could ask what role transcriptional load plays in DNA damage. A third possibility is that R-loop induced

rDNA instability is a specific result of RNA pol I transcription. Using an RNA pol II based rDNA transcription system will allow us to dissect pol I functions.

Lastly, it is as yet unclear which mechanism repairs foci in the absence of BIR. The ability of the *PIF1-E467G* allele to encourage non-BIR repair events after a DSB might be crucial in allowing the repair of damage events in *rnh1*Δ *rnh201*Δ *top1*Δ cells. Alternatively, given the abundance of homology in the highly repetitive rDNA locus, it is possible that single-strand annealing (SSA) or a GC pathway takes over.

This study sheds new light on the functions of the RNases H in maintaining genome stability. A primary role for hybrid removal systems now appears to be preventing BIR from occurring at highly transcribed repetitive elements such as the ribosomal locus. Given the high conservation of the RNases H and the pervasiveness of transcribed repetitive elements in larger mammalian genomes, we suspect that these results could have broad implications for genome stability in many organisms.

Appendix I. Details on genetic screen

Chapter II of this dissertation discussed results from a genetic screen for spontaneous suppressors of *rnh1*Δ *rnh201*Δ *top1*Δ lethality. Unfortunately, due to the time constraints, we were only able to follow up on the most promising and immediately exciting hits from the screen. These hits, *RPA190-KT, RPA190-V1486F,* and *PIF1-E467G* were found in four suppressor strains. *RPA190-V1486F* was found in two suppressors, but due to how the screen was performed, it is possible that these two suppressors were clonal. We therefore have 20 remaining suppressors for which we have sequencing data but for which no causative mutation has been identified. Additionally, there are suppressors that were not sequenced, either because we decided to only multiplex 24 libraries or because they grew extremely poorly and were therefore difficult to work with and more likely to gain secondary mutations. For future reference, raw sequence data, assembled genomes, identified SNPs, and notes on assembly can be found on the Mac Pro in a folder titled "Amon." For convenience, suppressors, SNPs, and progress made in identifying linkage are listed and cross-indexed here.

Table 1 – Suppressor strain names, adapter indices, and sequencing status. JA287 suppressors came from independent cultures outgrown at 30°C followed by growth on 5-FOA at 30°C, while these steps were performed at 23°C for JA288 strains. This was done to allow for the capture of temperature sensitive suppressors, but ultimately none were found. Both JA287 and 288 suppressors were collected from four separate outgrowth cultures. That is, JA271a (the parent strain for the screen) was grown on –URA and eight colonies were picked and used to inoculate eight YPD (non-selective) cultures, four grown at 30°C (JA287 strains) and four grown at 23°C (JA288 strains). These outgrowth cultures are numbered 1 through 4 and listed in this table. This is important to note, since multiple suppressors from a single outgrowth culture have the possibility of being clonal (*RPA190-V1486F* as an example). Strains carrying the three confirmed suppressors discussed in chapter II are bolded.

Strain	Outgrowth culture	Sequenced?	Adapter index
JA271a	parent	yes	27
JA287a	1	yes	1
JA287b	1	yes	2
JA287c	1	yes	3
JA287d	1	yes	4
JA287e	1	yes	5
JA287f	2	yes	6
JA287g	2	no, slow growth	
JA287h	2	yes	7
JA287i	2	yes	8
JA287j	2	yes	9
JA287k	3	yes	10
JA287l	3	yes	11
JA287m	3	yes	12
JA287n	3	no	-
JA287o	3	no	-
JA287p	4	no	-
JA287q	4	no	-
JA287r	4	no	-
JA288a	1	yes	13
JA288b	1	yes	14
JA288c	1	no, slow growth	-
JA288d	1	yes	15
JA288e	1	yes	16
JA288f	2	no, slow growth	-
JA288g	2	no, slow growth	-
JA288h	2	yes	18
JA288i	2	yes	19
JA288j	2	yes	20
JA288k	3	yes	21
JA288l	3	yes	22
JA288m	3	yes	23
JA288n	3	yes	25
JA288o	3	no	-
JA288p	4	no	-
JA288q	4	no	-
JA288r	4	no	-
JA288s	4	no	-

All mutations found are listed below in Table 2. It was later discovered that a surprising number of mutations appeared to be secondary. After suppressor strains were isolated and their phenotypes were confirmed, they were first frozen at -80°C for storage. Individual colonies were then used to start fresh cultures for isolating genomic DNA for whole-genome sequencing. Some mutations found by whole-genome sequencing were not present when PCR-sequenced from colonies grown from -80°C stocks. These mutations were not an artifact of any sequencing step, as they were confirmed to be present in genomic DNA stocks used to prepare libraries. These secondary mutations therefore most likely arose in the outgrowth step used to collect enough cells for genomic DNA extractions. The column "primary?" refers to whether or not the mutation was found in the original suppressor strain. An empty value in this column means that the mutation has not been checked - for these strains, mutations need to be confirmed before any linkage experiments are performed. Suppressors carrying primary mutations were crossed to *MAT*-alpha strain JA290a (*rnh1*Δ *rnh201*Δ *top1*Δ *pRNH1*) and subsequently sporulated. Tetrads were dissected and then PCR-sequenced at the locus of the mutation. All primary mutations segregated 2:2. The column "linked?" refers to analysis of these tetrads. "No" in this column means at least one spore segregated with the mutation, was *rnh1*Δ *rnh201*Δ *top1*Δ, had lost the *RNH1* plasmid, and was inviable. "Yes" in this column, which only applies to the three suppressors discussed in chapter II (bolded), means that 5 viable spores were found with the mutation, were *rnh1*Δ *rnh201*Δ *top1*Δ, and had lost the *RNH1* plasmid. Since these mutations segregated independently from all other markers of interest, this gave us about 97% confidence that the they were linked to the suppression phenotype. This was high enough confidence to proceed with strain construction for confirming linkage.

Table 2 – List of mutations indexed by strain. Strains had between one and eight alterations when compared to the parent strain JA271a. The genes that these mutations correspond to are listed here, along with the protein coding change (if applicable – syn., synonymous substitution), chromosome location, and mutation. SNPs were mapped to S288c reference sequence R64-1-1 last modified on February 3, 2011. Note that all mutations listed are transitions and transversions – all larger mutations and insertions/deletions were filtered out in the SNP calling process. It is likely that some causative mutations have been missed due to this filtering.

Strain	Gene and alteration	Chr.	Position	Mutation	Primary?	Linked?
JA287a	*HLR1-S387T*	IV	1495745	C > A		
	CLB4-A350S	XII	563055	G > T	no	
	no feature	XIV	64711	T > A		
JA287b	no feature	V	53892	A > C		
	CPR7-F261L	X	491863	C > G		
	IML1-K760R	X	686845	A > G		
	no feature	XI	650671	G > C		
	IMP4-D59N	XIV	485781	G > A	yes	no
JA287c	*LCP5 syn.*	V	414630	C > T		
	DNF1-L792M	V	515117	C > A		
	no feature	VIII	493707	G > A		
	YIL067C-S572Y	IX	236046	G > T	no	
	FAR8 syn.	XIII	330066	A > G		
JA287d	*YSA1-L11V*	II	461843	G > C		
	YHR097C syn.	VIII	297923	G > A		
	MLP2-K219R	IX	67412	T > C		
	TOF2-D107N	XI	460921	C > T	no	
	ECI1 syn.	XII	706522	C > A		
	SIN3 syn.	XV	318551	G > A		
JA287e	*no feature*	XII	52783	C > G		
	EST2-T842I	XII	769066	C > T	yes	no
	PDS5-N902E	XIII	417326	T > C	yes	no
JA287f	*TFC3-G745V*	I	148844	C > A	no	
	STE5-A436G	IV	659656	C > G		
	YAP7-A198S	XV	270779	C > A	yes	no
	PRE2-D193H	XVI	732925	G > C		
JA287h	*MRPL36 syn.*	II	484048	G > A		
	no feature	III	246784	A > G		
	UTP22-P941R	VII	665179	C > G		
	tRNA	VIII	133024	A > G		
	YJL132W syn.	X	161967	T > C		
	ANR2-A472V	XI	350877	C > T		
	RFX1-P201S	XII	509632	G > A	no	
	RPA190-V1486F	**XV**	**965442**	**G > T**	**yes**	**yes**
	DBP1 syn.	XVI	326255	A > G		
	COG4 syn.	XVI	738979	C > A		
JA287i	*VAM6-H8L*	IV	320098	T > A		
	no feature	V	555027	T > G		

	no feature	VIII	108210	C > T		
	LAA1 syn.	X	44245	C > T		
	RAD5-Q248E	XII	205732	C > G	no	
	BCH1-A470S	XIII	745156	G > T		
	VIK1 syn.	XVI	71945	C > T		
JA287j	*tRNA*	VIII	133024	A > G		
	no feature	XV	550681	A > C		
	RPA190-V1486F	**XV**	**965442**	**G > T**	**yes**	**yes**
	no feature	XVI	132563	G > C		
	YOK062W-C97F	XVI	432184	G > T		
JA287k	*no feature*	IV	512432	C > T		
	no feature	V	238088	A > T		
	no feature	XII	634184	G > T		
	RRN9-L252F	XIII	805668	T > A	no	
	no feature	XV	94675	C > G		
	OPT2-I286F	XVI	926082	T > A		
JA287l	*SAC6-G242R*	IV	714545	C > G		
	FYV4-M1I (no start)	VIII	220110	G > A	no	
	RTC1-D239Y	XV	64636	C > A		
JA287m	*PRP8-A459S*	VIII	435574	C > A	no	
	no feature	XI	329547	A > G		
	VIP1-K278N	XII	938674	A > C		
	dubious ORF	XII	954638	C > G		
JA288a	*no feature*	VII	310699	A > C		
	dubious ORF	VII	592948	G > T		
	IMP4 syn.	XIV	485870	C > T		
	RPA190-K1482T	**XV**	**965431**	**A > C**	**yes**	**yes**
JA288b	*PIB2-E58ochre*	VII	451933	C > A	no	
	no feature	X	265182	G > T		
JA288d	*no feature*	II	134136	A > C		
	TPS1-G353opal	II	489336	C > A		
	SEH1-R277I	VII	314063	G > T		
	GLG1-L245F	XI	553504	G > T		
JA288e	*no feature*	V	151167	C > G		
	DAP2-V11L	VIII	167382	G > C		
	SMF3-G204C	XII	211324	C > A	no	
JA288h	*FUI1-R125I*	II	139887	C > A	yes	no
	TAO3 syn.	IX	110121	C > A		
	HOS4-N656K	IX	153562	C > A		
	ALT1-Q248E	XII	318347	G > T		
	no feature	XII	320307	A > C		

JA288i	*UFD2-D513E*	IV	120054	A > C	no	
	no feature	XIII	698537	G > T		
	no feature	Mito.	45145	A > T		
JA288j	*no feature*	IV	1188997	G > A		
	CEM1-D138E	V	279213	G > T		
	LST4-W318amber	XI	117034	C > T		
	YLL054C-S797P	XII	32816	A > G	yes	no
JA288k	*no feature*	X	576615	C > T		
	PIF1-E467G	**XIII**	**150133**	**T > C**	**yes**	**yes**
JA288l	*PWP2 syn.*	III	221888	G > A		
JA288m	*RSC1 syn.*	VII	602248	T > G		
	DAP2-V11L	VIII	167382	G > C		
	NDD1-S532C	XV	1034877	G > C	yes	no
	TCO89-Q291ochre	XVI	206118	C > T		
JA288n	*CTR86-D423V*	III	218800	T > A	yes	no
	CUL3 syn.	VII	500599	G > C		
	no feature	XI	321598	C > T		
	RFX1-T500A	XII	508735	T > C	yes	no
	MKS1-S359opal	XIV	484631	C > G		
	SSK2-V1391I	XIV	681263	C > T		